

Article

Discovery of Novel Indole-based Allosteric Highly Potent ATX Inhibitors with Great *in vivo* Efficacy in Mouse Lung Fibrosis Model

Hongrui Lei, Ming Guo, Xiaopeng Li, Fang Jia, Changtao Li,
Yu Yang, Meng Cao, Nan Jiang, Enlong Ma, and Xin Zhai

J. Med. Chem., **Just Accepted Manuscript** • DOI: 10.1021/acs.jmedchem.0c00506 • Publication Date (Web): 01 Jun 2020

Downloaded from pubs.acs.org on June 1, 2020

Just Accepted

“Just Accepted” manuscripts have been peer-reviewed and accepted for publication. They are posted online prior to technical editing, formatting for publication and author proofing. The American Chemical Society provides “Just Accepted” as a service to the research community to expedite the dissemination of scientific material as soon as possible after acceptance. “Just Accepted” manuscripts appear in full in PDF format accompanied by an HTML abstract. “Just Accepted” manuscripts have been fully peer reviewed, but should not be considered the official version of record. They are citable by the Digital Object Identifier (DOI®). “Just Accepted” is an optional service offered to authors. Therefore, the “Just Accepted” Web site may not include all articles that will be published in the journal. After a manuscript is technically edited and formatted, it will be removed from the “Just Accepted” Web site and published as an ASAP article. Note that technical editing may introduce minor changes to the manuscript text and/or graphics which could affect content, and all legal disclaimers and ethical guidelines that apply to the journal pertain. ACS cannot be held responsible for errors or consequences arising from the use of information contained in these “Just Accepted” manuscripts.

Discovery of Novel Indole-based Allosteric Highly Potent ATX Inhibitors with Great *in vivo* Efficacy in Mouse Lung Fibrosis Model

Hongrui Lei^a, Ming Guo^a, Xiaopeng Li^b, Fang Jia^a, Changtao Li^a, Yu Yang^a, Meng Cao^a, Nan Jiang^a, Enlong Ma^{b*}, Xin Zhai^{a*}

^aKey Laboratory of Structure-Based Drug Design and Discovery, Ministry of Education, Shenyang Pharmaceutical University, Shenyang 110016, China.

^bDepartment of Pharmacology, Shenyang Pharmaceutical University, Shenyang 110016, China.

Abstract

Autotaxin (ATX) is the dominant catalytic enzyme accounting for the lipid mediator lysophosphatidic acid (LPA) through hydrolysis of lysophosphatidylcholine (LPC). There is great interest in developing non-acidic ATX inhibitors with specific binding mode to serve as potential *in vivo* effective therapeutic tools. Herein, dating from an HTS product **Indole-1** (740 nM), a dedicated optimization campaign was implemented through derivatizing the -COOH group to versatile linkers that well bridged the indole skeleton and the hydrophobic pocket binding groups. Ultimately, it was established that the coexistence of carbamate linker and a -OH group containing amines could generally furnish excellent indole based ATX inhibitors with even below 1 nM *in vitro* activities. Two optimal entities were advanced to a bleomycin induced mice pulmonary fibrosis model which exerted promising efficacy in alleviating the damaged lung texture caused by bleomycin exposure. The novel carbamate-containing indole based ATX inhibitors with concrete binding mode may contribute to the identification of potential therapeutic agents to intervene the fibrotic diseases.

Introduction

Lysophosphatidic acid (LPA) is a bioactive serum-borne lipid mediator which exerts its physiological effect through acting on specific G-protein coupled receptors (GPCRs) LPAR₁₋₆.¹ Accumulating evidence suggests that downregulation of LPA signaling has been proven effective in various diseases, such as tumor metastasis,^{2,3} fibrosis,⁴⁻⁶ pruritis,⁷ multiple sclerosis,⁸ inflammation⁹ and so on. Typically, autotaxin (ATX) turns out to be the predominant enzyme accounting for physiological source of extracellular LPA through a lysophosphatidylcholine (LPC) hydrolysis process (Figure 1).^{10,11}

ATX is the sole member of ectonucleotide pyrophosphatase/phosphodiesterase family (ENPPs) that harbors lysoPLD/ATX activity over lysophospholipids.¹² Structurally, ATX is composed of two *N*-terminal somatomedin B (SMB)-like domains, a central catalytic phosphodiesterase (PDE) domain and an inactive nuclease-like domain.¹³ The catalytic bis-Zinc site is connected by a T-junction to a hydrophobic pocket and a partial “hydrophobic tunnel” (Figure 2).¹⁴ The tunnel referred to as the allosteric site binds steroid molecules, as well as the LPA product, which results in a modulation of ATX

catalytic efficiency¹⁴, while the hydrophobic pocket is designated the orthosteric site.¹⁵

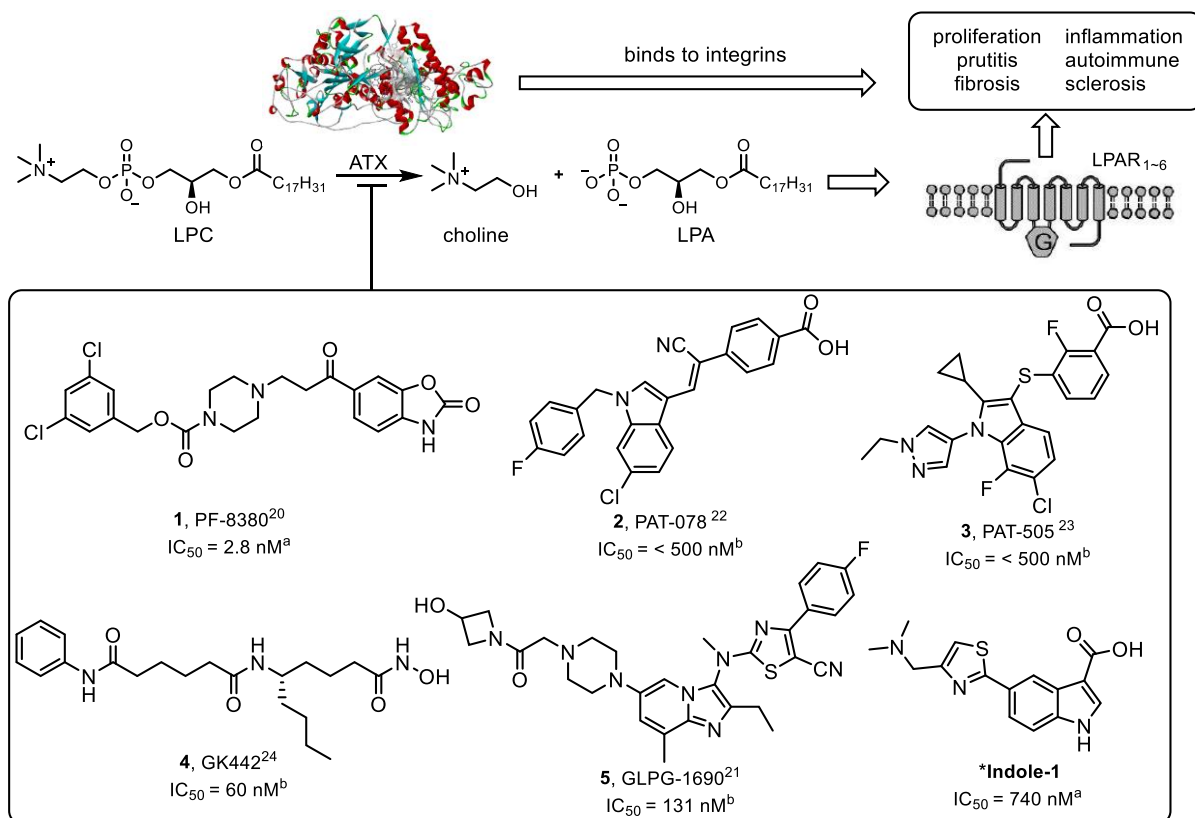


Figure 1. Function of ATX and uncovered ATX inhibitors. ^aFS-3 assay; ^bLPC choline release assay; *Our screening lead.

Taken together, ATX is endowed with the dual roles as an LPA producer and carrier, transporting LPA to distal sites from where LPC can be taken.¹⁶ Initially, classical ATX inhibitors derived from lipid analogues shared great similarities with sphingosine-1-phosphate (S1P) or LPA. With the massive research in depth, ATX inhibitors with distinct chemical properties were designed which included lipid-based inhibitors,¹⁷ DNA aptamers,¹⁸ as well as small molecules.^{15,19-20} Furthermore, small molecules can be in turn classified in four distinct types (I, II, III and IV) depending on their mode of binding to the ATX tripartite site.¹⁵

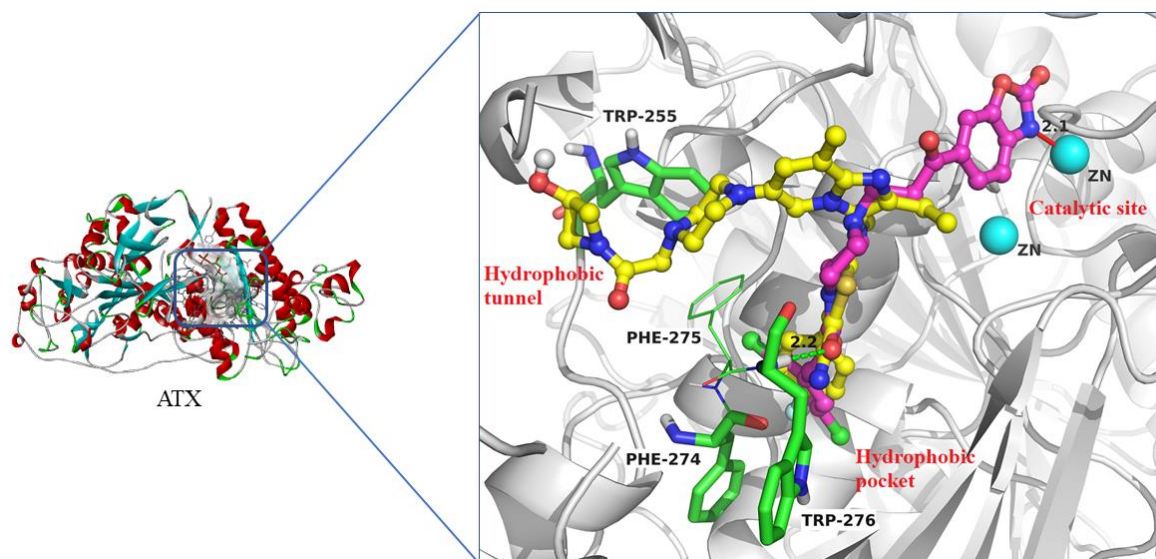


Figure 2. Structure and active site of ATX. Type I inhibitor PF-8380 (magenta stick) and type IV inhibitor GLPG-1690 (yellow stick) were superimposed in the active site (The H-bond was indicated in green dash line while the covalent interaction was shown in red line).

Typically, PF-8380²¹ (binds the hydrophobic pocket and the catalytic site, **1**) and GLPG-1690²² (binds the hydrophobic pocket and the tunnel, **5**) were known as the representative type I and type IV ATX inhibitors, which shared a great uniformity in binding modes within the hydrophobic pocket. However, PF-8380, as well as the type II (binds the hydrophobic pocket, **2**²³) and type III (binds the hydrophobic tunnel, **3**²⁴) entities²⁵ featuring an acidic head suffered from poor druggability with none of inhibitors entering clinical trials. Recently, a δ -norleucine based hydroxamic acid derivative GK442²⁶ (**4**) was tested *in vivo* effects in bleomycin (BLM)-induced mice lung fibrosis model with moderate protecting effects. However, to date, the sole candidate in clinical trial was the type IV inhibitor GLPG-1690 (Ziritaxestat) developed by Galapagos, which was proved efficacious to reduce extracellular matrix deposition in the pulmonary fibrosis model.^{22, 27-29} Typically, the type IV inhibitors could preclude the binding of bile acid and LPA derivatives to ATX by occupying both the hydrophobic tunnel and the hydrophobic pocket, avoiding any interactions of substrates with the zinc atoms. Whereas all types of ATX inhibitors block the formation of LPA, type IV inhibitors could also prevent LPA transport and delivery to LPA receptors through ATX channel occupancy. The advantages mentioned above of type IV ATX inhibitors may provide a rationale for their predominant prospect in ATX-LPA axis related diseases.

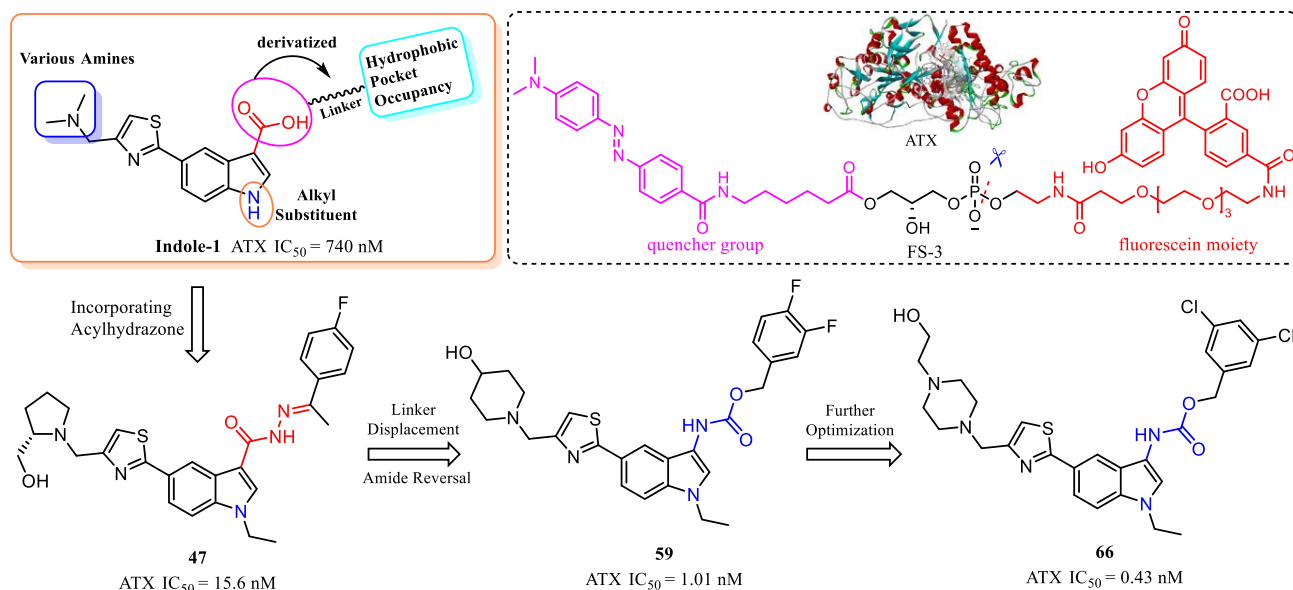


Figure 3. Structure optimization process of indole-based ATX inhibitors.

Through a FS-3 based high throughput screening effort, an indole-3-carboxylic acid lead **Indole-1** was identified (ATX IC_{50} : 740 nM). In pursuit of developing non-acidic type IV inhibitors, the carboxylic group was modified to achieve an efficient occupancy of the hydrophobic pocket. Meanwhile, the tiny dimethylamine fragment was altered to various amines to explore the possible interactions within the hydrophobic tunnel. Herein, optimization and structure-activity relationships (SARs) of novel indole-based ATX inhibitors with high *in vitro* enzymatic activities and impressive *in vivo* effectiveness in BLM-challenged mice pulmonary fibrosis model was described.

Results and Discussion

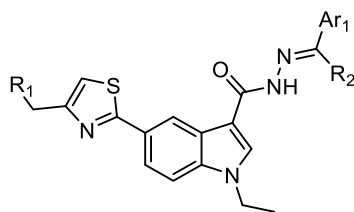
Starting from the HTS hit **Indole-1**, we conducted a systematic SARs-based optimization campaign in pursuit of acquiring *in vivo* effective allosteric highly potent ATX inhibitors. As there was great interest to focus on non-acidic entities as novel ATX inhibitors for specific binding mode and promising druggability, the -COOH group of **Indole-1** was derivatized in search of a highly tolerable linker that well bridged the indole skeleton and the hydrophobic pocket binding moieties.

***In vitro* ATX inhibition assay: Structure-Activity Relationships and binding mode Studies.** All synthesized indole-based derivatives were tested for their *in vitro* inhibition effect on recombinant mouse ATX using the Amplex Red PLD assay kit (Echelon Biosciences, Inc. Salt Lake City, UT). FS-3 was used as substrate, and the inhibition results are presented in Tables 1~4. The molecular weight (MW), cLogP and PSA of the new synthetic compounds predicted using ChemOffice Ultra or corresponding websites³⁰ were included in the Tables. The ligand lipophilicity efficiency (LLE) values of the chemical entities were calculated according to the IC_{50} values and the cLogP values obtained. It should be stated that a positive (+) LLE value was highly preferred for a promising entity.³¹⁻³² The parameters above are important properties

of target compounds which may provide essential information for the evaluation of druggability.

Incorporation of the Acyl hydrazone linker. Firstly, the acyl hydrazone was taken into consideration as a potential linker connecting the indole skeleton and the hydrophobic pocket binding moieties. To this end, the carboxylic acid group in **Indole-1** was derivatized to the corresponding acyl hydrazones, and the dimethylamine group in **Indole-1** was replaced by various secondary amines with expanded volume for an efficient occupancy of the hydrophobic tunnel. An ethyl group was introduced on position-1 of the indole core as an initial attempt to better fit the protein region. First of all, morpholine containing compounds (**20~23**) were explored with the aldehydes/ketones fixed to 4-fluoro benzaldehyde (**20**), 4-methoxy benzaldehyde (**21**), piperonal (**22**) and 4-fluoroacetophenone (**23**). Generally, four compounds did not exert ATX inhibitory activities superior to **Indole-1** (740 nM). It seemed that electron-withdrawing groups on the aldehyde/ketones in **20** (1370 nM) & **23** (1840 nM) presented a primary affinity over the electron-donating groups in **21** (>10000 nM) and **22** (>10000 nM).

Table 1. FS-3 Based *In Vitro* Inhibitory Activities of Compounds 20~35 against ATX



Compd.	R ₁	R ₂	Ar ₁	MW	cLogP	PSA	LLE	IC ₅₀ ^a (nM) ±SD ^b
Indole-1	-	-	-	301.09	2.47	52.63	2.66	740±27
20		H		491.18	4.68	59.15	0.18	1370± 81
21		H		503.20	4.50	66.70	<-0.50	>10000
22		H		517.18	4.56	76.27	<-0.56	>10000
23		-CH ₃		505.19	4.65	58.44	0.09	1840 ± 170
24		H		489.20	6.00	51.24	-1.60	3960 ± 213
25		H		515.20	5.88	68.36	-1.07	1550 ± 170
26		H		487.20	5.46	59.15	-0.62	1460 ± 145
27		H		491.15	6.08	51.61	-1.15	1170 ± 127
28		-CH ₃		489.20	5.61	50.90	-1.05	2740 ± 154
29		-CH ₃		518.23	4.70	71.84	-0.10	2530 ± 230

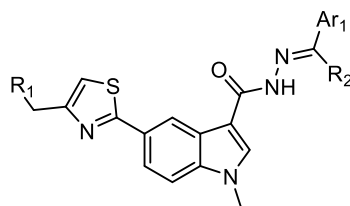
30		H		530.21	4.61	54.01	0.51	757 ± 45
31		H		503.22	6.26	51.24	<-2.26	>10000
32		H		529.21	6.14	68.36	<-2.14	>10000
33		H		518.23	5.22	54.78	-0.35	1349 ± 98
34		H		534.20	5.67	54.78	-1.03	2310 ± 131
35		-CH ₃		532.24	5.19	54.07	-0.39	1590 ± 95
PF-8380	-	-	-	477.09	3.80	73.50	3.77	2.7 ± 0.32
GLPG-1690	-	-	-	588.24	3.84	77.96	4.05	1.3 ± 0.11

^adata were the results in at least two independent assays.

However, once morpholine was altered to piperidine, pyrrolidine and *N*-methyl piperazine, the tendency was vanished. For example, the 4-F-phenyl containing **24** (3960 nM), **28** (2740 nM) and **29** (2530 nM) performed worse than the corresponding alkyloxy phenyl derivatives **25** (1550 nM), **26** (1460 nM) and **30** (757 nM), especially, **30** performed similar potency with **Indole-1**. In view of the atom volume, there was no clear trend between the F- and Cl-containing compounds, such as **27** (2740 nM) vs **26** (1170 nM) and **33** (1349 nM) vs **34** (2310 nM). The 4-methyl piperidine derivatives **31** and **32** exerted IC₅₀s over 10000 nM perhaps due greatly to the highly hydrophobic property of the 4-methylpiperidine ring. As expected, the *N*-ethyl piperazine compounds (**33**~**35**) were detected similar ATX inhibition potency with the counterpart **29**~**30** bearing *N*-methyl piperazine. In the meantime, the utilization of aldehyde or ketone may exert no obvious influence in activity for that the 4-fluoro benzaldehyde products presented parallel enzymatic profile with 4-fluoroacetophenone (**20** vs **23** or **33** vs **35**). Taken together, the first trial may turn out to be a frustrating attempt with only micromolar activities achieved. Hence, further modifications were put on agenda.

Exploring the indole N-alkyl substituent. The preliminarily involvement of the 1-indole ethyl resulted to be a temporary expedient which may be a potential sally port for the following research. Generally, the former uncovered ATX inhibitors bore no active hydrogens in the skeleton section.¹⁵ Hence, the primary ethyl group was replaced with a more versatile methyl which led to the design and synthesis of **36**~**38** as well as **39**~**41**. The morpholine and *N*-methyl piperazine with relatively better potency above were selected as the reference amines.

Table 2. FS-3 Based *In Vitro* Inhibitory Activities of Compounds 36~41 against ATX



Compd.	R ₁	R ₃	Ar ₁	MW	cLogP	PSA	LLE	IC ₅₀ ^a (nM) ±SD ^b
36		H		477.16	4.21	59.98	0.33	2870 ± 211
37		H		493.13	4.66	59.98	<-0.66	>10000
38		H		503.16	4.10	77.10	<-0.10	>10000
39		H		490.20	4.27	55.55	0.01	5240 ± 342
40		-CH ₃		504.21	4.24	54.84	<-0.24	>10000
41		H		516.19	4.15	72.67	0.91	879 ± 77

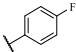
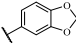
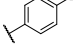
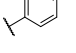
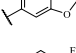
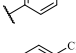
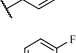
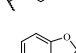
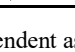
^adata were the results in at least two independent assays.

However, much to our disappointment, the 1-methyl derivatives (**36**, **39** and **41**) exerted a little weaker potency relative to the corresponding **20**, **29** and **30**. Even more frustrated, **37**, **38** and **40** were detected loss of ATX inhibition effect. These results suggested that the substituent on position-1 may not be a key factor for an efficient promotion of the activity. Therefore, we retained the preliminarily tolerated ethyl group for the following identification.

Introduction of -OH containing amines. Given our hypothesis that the aliphatic amines stretched to the hydrophobic tunnel or even exposed to the solvent region, the nature of the amine itself may account a lot for the binding affinity with ATX. In this sense, we further introduced the -OH containing amines to the chloromethyl thiazole moiety in pursuit of acquiring more efficient inhibitors. Subsequently, compounds **42**~**45**, **46**~**48** and **49**~**52** were synthesized with the same procedure as **20**~**41**.

Table 3. FS-3 Based *In Vitro* Inhibitory Activities of Compounds 42~52 against ATX

Compd.	R ₁	R ₂	R ₃	MW	cLogP	PSA	LLE	IC ₅₀ ^a (nM) ±SD ^b
42		H		505.19	4.22	66.97	0.82	906±121.0
43		H		521.17	4.63	66.97	1.11	180±27.0

44	-CH ₃		519.21	3.79	66.25	2.37	69.4±4.5
45	H		531.19	3.85	84.08	2.12	107.4±17.0
46	H		505.19	4.57	68.54	0.61	655±65.0
47	-CH ₃		519.21	4.14	67.83	2.66	15.7±1.1
48	H		531.19	4.19	85.65	1.02	610 ±47.0
49	H		534.22	4.06	71.69	1.81	134.9±13.8
50	H		550.19	4.43	71.69	1.21	231.1 ±25.3
51	-CH ₃		548.24	4.03	70.98	1.26	507.9±31.5
52	H		560.22	3.94	88.81	0.94	1320± 127.0

^adata were the results in at least two independent assays.

Surprisingly, except for **45** (IC₅₀ =1320 nM), the -OH containing analogs **42~52** exerted sub-micromolar IC₅₀ values or even better. Among these, **44** and **47** were detected as the most potent ATX inhibitors with IC₅₀ values of 69.4 nM and 15.7 nM, respectively. Given the obvious improvement in activities, we performed a docking study using the 3D template of **47** with the cocrystal structure of ATX (5MHP),²¹ and the computational results were presented in Figure 4.

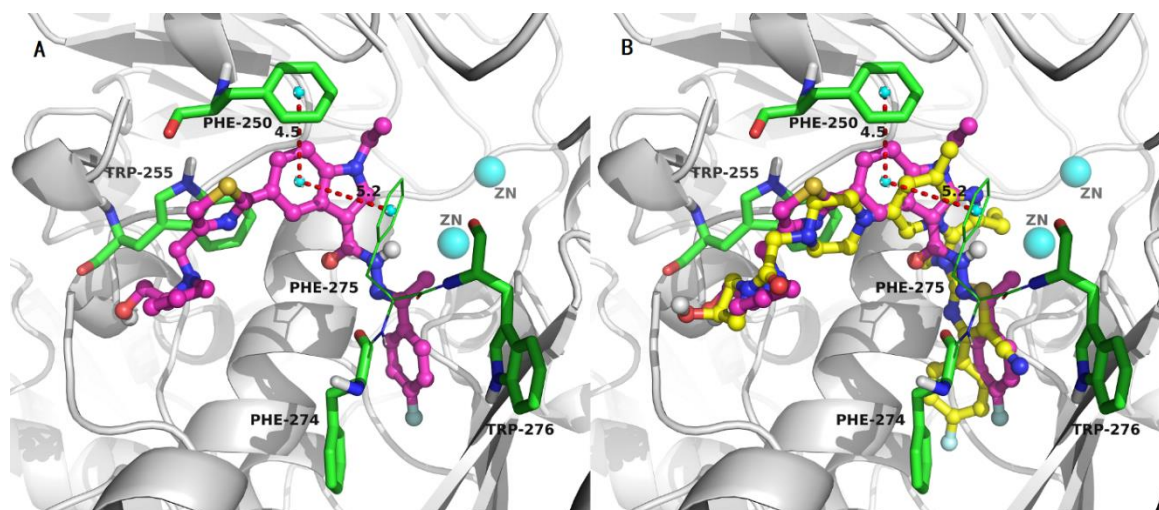


Figure 4. (A) Binding mode of **47** with ATX; (B) Overlapping of **47** with GLPG-1690 within the active site of ATX.

As shown in Figure 4A, the indole skeleton made two essential π - π interactions with residues Phe250 and Phe275. Meanwhile, another key π - π interaction was observed between the thiazole ring of **47** and Trp255. The prolinol moiety did stretch into the solvent region through the hydrophobic tunnel. As expected, the acyl hydrazone linker typically bridged the indole skeleton and the 4-fluorophenyl group and directed the 4-fluorophenyl group to the hydrophobic pocket formed by Phe274-Phe275-Trp276 and other residues. In Figure 4B, **47** and GLPG-1690 were superimposed within the active site

of ATX. It was apparently shown that **47** adopted a quite similar pose with the reference GLPG-1690. However, mainly due to the rigid carbonyl group in the acyl hydrazone moiety, the 4-fluorophenyl group was away from (perpendicular to) the 4-fluorophenyl moiety in GLPG-1690 which may account for a poor occupancy of the hydrophobic pocket. This virtual docking offered a potential rationale for the difference between **47** and GLPG-1690 (15.7 nM vs 1.3 nM).

The amide bond reversal leading to carbamate analogues with -OH containing amines. The apparent enhanced potency of **47** encouraged us greatly for a new stage of modification. Given the rigidity property of the carbonyl group on 3-position of indole backbone, it was hypothesized to conduct an amide bond reversal strategy to yield flexible linkers. Ultimately, the versatile carbamate moiety was recommended as a surrogate for the former acyl hydrazone (Figure 5). Various benzyl alcohols were introduced to implement a condensation reaction following the Curtius rearrangement reaction of indole-3 carboxylic derivatives.

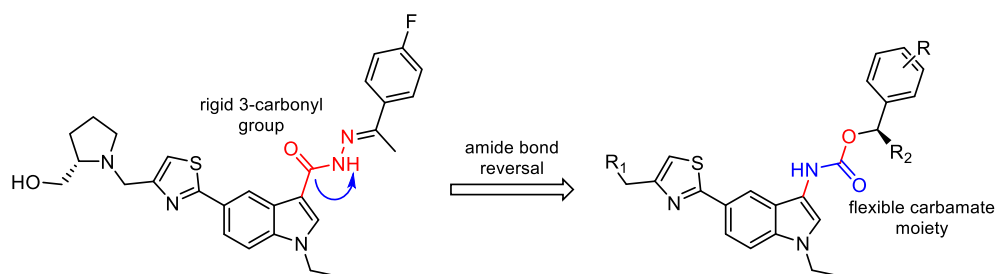


Figure 5. Amide bond reversal strategy to transform the acyl hydrazone group to the carbamate linker.

According to the SARs above, the well tolerated -OH containing amines, prolinol, 4-OH piperidine, *N*-hydroxyethyl piperazine as well as diethanolamine were explored firstly. Among the 4-OH piperidine derivatives (**53**~**59**), **53**~**57** were detected sub-micromolar IC₅₀ values ranging from 117 nM to 970 nM. It was noteworthy that the unsubstituted phenyl group **55** (970 nM) performed worse than others. **58** with a 1,3-benzodioxole moiety exerted even better activity (34.1 nM) although an unfavorable drug-likeness score (0.92) was obtained. To our great surprise, the 3,4-difluoro derivative **59** displayed 1.01 nM activity which may suggest a considerable breakthrough. In view of the impressive potency of **59**, we performed a detailed virtual docking between **59** and ATX (Figure 6).

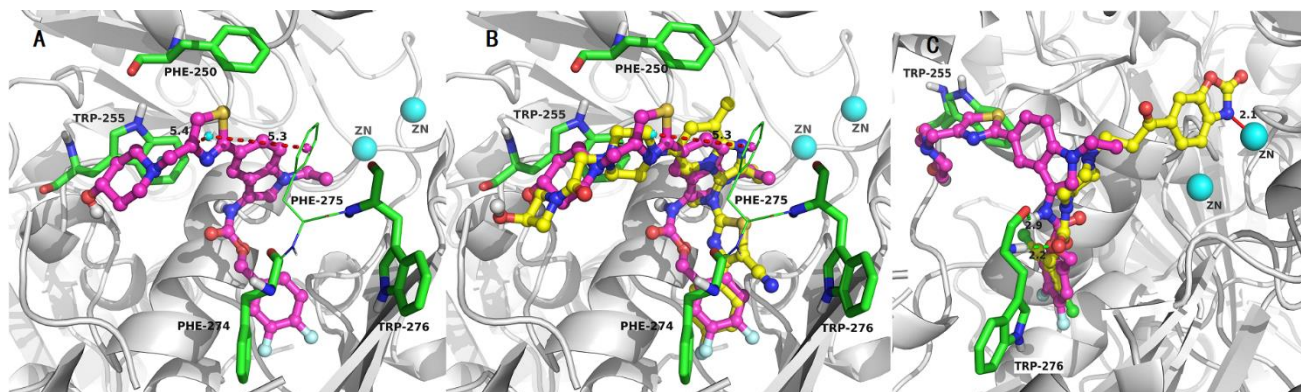


Figure 6. (A) Binding mode of **59** with ATX; (B) Overlapping of **59** with GLPG-1690 within the active site of ATX; (C) Overlapping of **59** with PF-8380 within the active site of ATX (The H-bonds/ π - π interactions were indicated in green/red dash lines while the covalent interaction was shown in red line).

As shown in Figure 6A, the thiazole ring and the indole skeleton of **59** produced similar π - π interactions as that in **47** with Trp255, Phe250 as well as Phe275. Importantly, in Figure 6B, although the carbamate moiety in **59** was away from the 5-cyano thiazole fragment in GLPG-1690, it could be obviously found that the 3,4-difluorophenyl group in **59** were almost overlapped totally with the 4-fluorophenyl counterpart. This may ideally account for the excellent enzymatic activity of **59** *in vitro*.

As a continuation, the 4-OH piperidine was replaced with *L*-prolinol which furnished **60**~**65**. Generally, **61** and **64** were detected promising ATX IC₅₀s around 35 nM which failed to exceed that of **59**.

Subsequently, the extended -OH containing amine *N*-hydroxyethyl piperazine with an extra chain was explored after the successfully synthesis of compounds **66** and **67**. To our great surprise, **66** (0.43 nM) was detected sub-nanomolar activities while **67** was 150 folds less potent (62.7 nM). This discrimination between the two compounds may result from the hindrance of the 2-Cl substituent in the benzyl carbamate moiety of **67**. To further verify the potential role of introducing *N*-hydroxyethyl piperazine, a dedicated computational docking was implemented with **66** as a template and the results were shown in Figure 7.

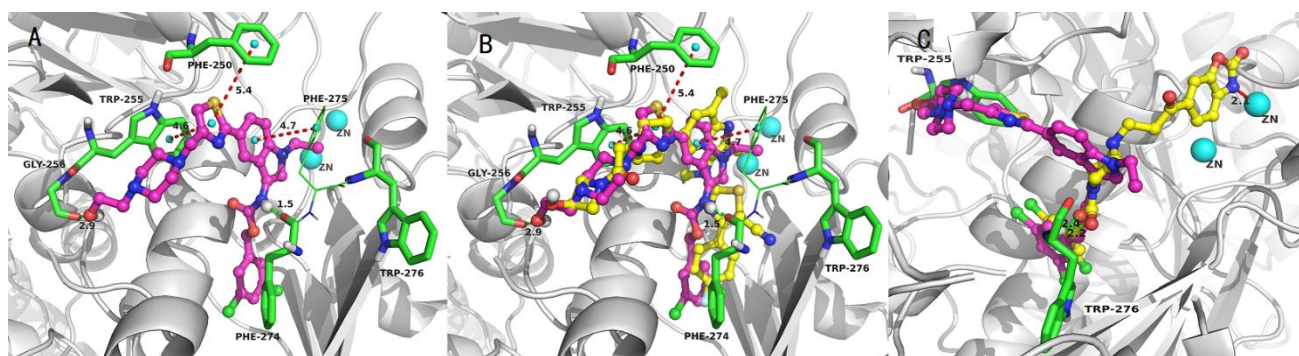
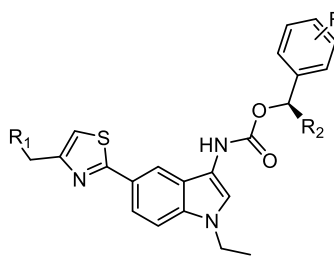


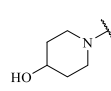
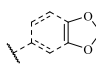
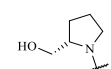
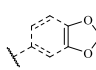
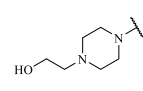
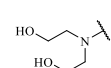
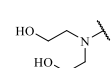
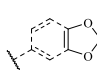
Figure 7. (A) Binding mode of **66** with ATX; (B) Overlapping of **66** with GLPG-1690 within the active site of ATX; (C) Overlapping of **66** with PF-8380 within the active site of ATX (The H-bonds/ π - π interactions were indicated in green/red dash lines while the covalent interaction was shown in red line).

Although the benzyl carbamate group in **66** was not thoroughly superimposed as that in **59** and the 4-fluorophenyl moiety in GLPG-1690, it did adopt a highly similar binding pose with the phenyl thiazole part in GLPG-1690. An essential 1.5 Å H-bond was detected between the carbamate NH- and Phe274 which greatly restrained the binding conformation of **66** within the hydrophobic pocket. It was noteworthy that the necessary H-bond was absent in **47** and **59**. Most importantly, the -OH group in **66** further approached the solvent region and formed a significant 2.9 Å H-bond with residue Gly256.

Taken together, the presence of two necessary H-bonds well explained the exceeding of **66** (0.43 nM) over GLPG-1690 (1.3 nM) in ATX inhibitory activity.

Table 4. FS-3 Based *In Vitro* Inhibitory Activities of Compounds 53~69 against ATX



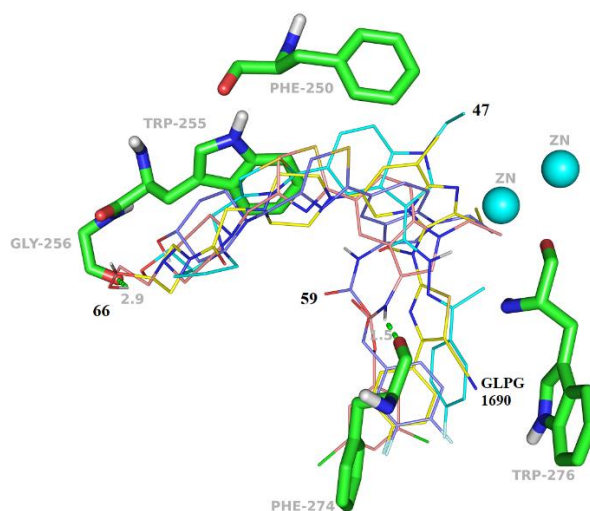
Compd.	R ₁	R	R ₂	MW	cLogP	PSA	LLE	IC ₅₀ ^a (nM) ±SD
53		3,5-di-Cl	H	558.13	6.05	62.50	-0.84	613±78.5
54		4-Me	-CH ₃	518.24	5.27	61.79	0.66	117± 21.7
55		H	H	490.20	4.62	62.50	0.39	970 ±45.1
56		2-Cl	-CH ₃	538.18	5.47	61.79	0.21	210 ± 17.1
57		2,3-di-Cl	H	558.13	5.81	62.50	0.09	127 ± 15.3
58			H	534.19	4.77	79.62	1.70	34.1 ± 2.1
59		3,4-di-F	H	526.19	5.04	62.50	2.96	1.01±0.2
60		H	H	490.20	4.53	64.07	1.38	121.8±13.1
61		4-Me	-CH ₃	518.24	5.19	63.36	1.24	36.9±5.3
62		2-Cl	-CH ₃	538.18	5.38	63.36	0.32	199.4±9.5
63		2,3-di-Cl	H	558.13	5.72	64.07	0.18	127.3 ± 8.7
64			H	534.19	4.68	81.19	1.78	34.7 ±4.5
65		3,4-di-F	H	526.19	4.95	64.07	0.58	297.2±31.7
66		3,5-di-Cl	H	587.15	5.27	67.22	3.10	0.43±0.05
67		2,3-di-Cl	H	587.15	5.03	67.22	1.17	62.7 ± 7.4
68		3,5-di-Cl	H	562.12	3.83	80.30	2.84	21.3±2.8
69			H	538.19	3.35	97.41	3.16	30.7±5.1

^adata were the results in at least two independent assays.

After identifying the pretty powerful -OH containing carbamate derivatives, we then synthesized **68** and **69** to develop

1
2
3
4 the possible effect of the number of -OH group. The enzymatic results that the diethanolamine finally furnished moderate
5
6 ATX inhibitory activities (**68** 21.3 nM, **69** 30.7 nM) suggested no regular pattern in the activity and the -OH count. In this
7
8 end, it could be preliminarily concluded that the combination of -OH containing amines, especially *N*-hydroxyethyl
9
10 piperazine, and the carbamate moiety generally provided the highly potent ATX allosteric inhibitors.

11
12 *Superimposing of 47, 59 and 66 with GLPG-1690 within the active site of ATX.* For an intuitive vision, the binding
13
14 poses of the representative compounds **47**, **59** and **66** were placed in the cocrystal structure of GLPG-1690 and ATX (Figure
15
16 8). Firstly, it could be easily seen that the benzyl carbamate moiety of **47** (cyan lines) was a little bit away from the exact
17
18 binding site of the hydrophobic pocket. Next, the amide reverse strategy from the acyl hydrazone did bring a highly flexible
19
20 linker carbamate. Although the carbamate fragment of **59** was twisted to some degree, its phenyl group surprisingly
21
22 achieved an utmost consistence with the benzene ring of GLPG-1690. Then, the -OH group in **66** stretched further
23
24 approaching the solvent region and formed a significant H-bond with Gly256. Finally, the principle H-bond between **66**
25
26 and Phe274 may turn out to be the marked contribution to its extra good *in vitro* enzymatic activities.



27
28
29
30
31
32
33
34
35
36
37
38
39
40
41
42
43
44
45 Figure 8. The binding mode of **47** (cyan lines), **59** (orange lines) and **66** (pink lines) superimposed with GLPG-1690 (yellow lines) within
46
47 ATX active site. (The hydrogen bonds were indicated in green dash lines).

48
49 To conclude, after a dedicated SARs-guided optimization, we identified a series of highly potent ATX inhibitors (sub-
50
51 nanomolar activities) with specific binding modes through efficiently interactions with the hydrophobic pocket and the
52
53 allosteric partial hydrophobic tunnel. It was envisioned that the combination of carbamate linker with a -OH containing
54
55 amines could offer a robust ATX inhibitory potency. We hope it works to promote the efficiency in identifying novel ATX
56
57 inhibitors through this discovery.

58
59 ***Ex vivo* ATX enzymatic assay and *In vivo* prophylactic effect of 59 and 66 on a Bleomycin-induced Mice**

1
2
3
4 **Pulmonary Fibrosis Model.** After verifying the *in vitro* enzymatic activities of target compounds (**59** and **66**), the next
5 stage was to evaluate their *in vivo* effects in inhibiting ATX activity. The BLM-induced pulmonary fibrosis model in rodents
6 turn out to be the principle animal model to examine the compounds as potential therapies for IPF.³³ It was well known
7 that the concentration and activity of ATX increase obviously which may account for the severity of fibrosis.³⁴ The
8 C57Bl/6J mice were undergone oral treatment with GLPG-1690 (60mg/kg) or compounds **59** and **66** (20 or 60 mg/kg)
9 once a day for 31 days (day -3 to day 28). After three days (day +1), the mice in test groups (5 mice per group) were
10 subjected to a tracheal administration of BLM to build the IPF model (Figure 9A). Meanwhile, the model group was treated
11 with saline as surrogate of the test compounds whereas the control group was the untreated mice with normal lung
12 textures.³⁵ Of note, death only occurred within the BLM model group (3 death in total). In the meantime, the body weight
13 changes of the mice were shown in Figure 9C and 9D. It was apparently that the test compounds (**59**, **66** and GLPG-1690)
14 could bring encouraging effects in protecting the BLM-treated mice with recovering of body weights. These results
15 preliminarily suggested a potential protective effect of the tested compounds on mice with injured lung tissues.
16
17
18
19
20
21
22
23
24
25

26
27 *Ex vivo* ATX enzymatic assay of **59** and **66** on a Bleomycin-induced Mice Pulmonary Fibrosis Model. The *ex vivo*
28 ATX lysoPLD activity was measured by the fluorescence excitation through the cleavage of the phospholipid bond in the
29 artificial substrate FS-3. A control sample was prepared to account for reference fluorescent absorption using 10 μ L lung
30 homogenate from the control group followed by addition of FS-3 substrate and the standard buffer. The relative absorbance
31 values were directly utilized for an intuitive analysis of the *ex vivo* ATX inhibitory effects of compounds **59**, **66** and GLPG-
32 1690. The lower absorbance value indicates a high inhibition of the *ex vivo* ATX activity. The results were shown in Figure
33 9B.
34
35
36
37
38
39
40
41
42
43
44
45
46
47
48
49
50
51
52
53
54
55
56
57
58
59
60

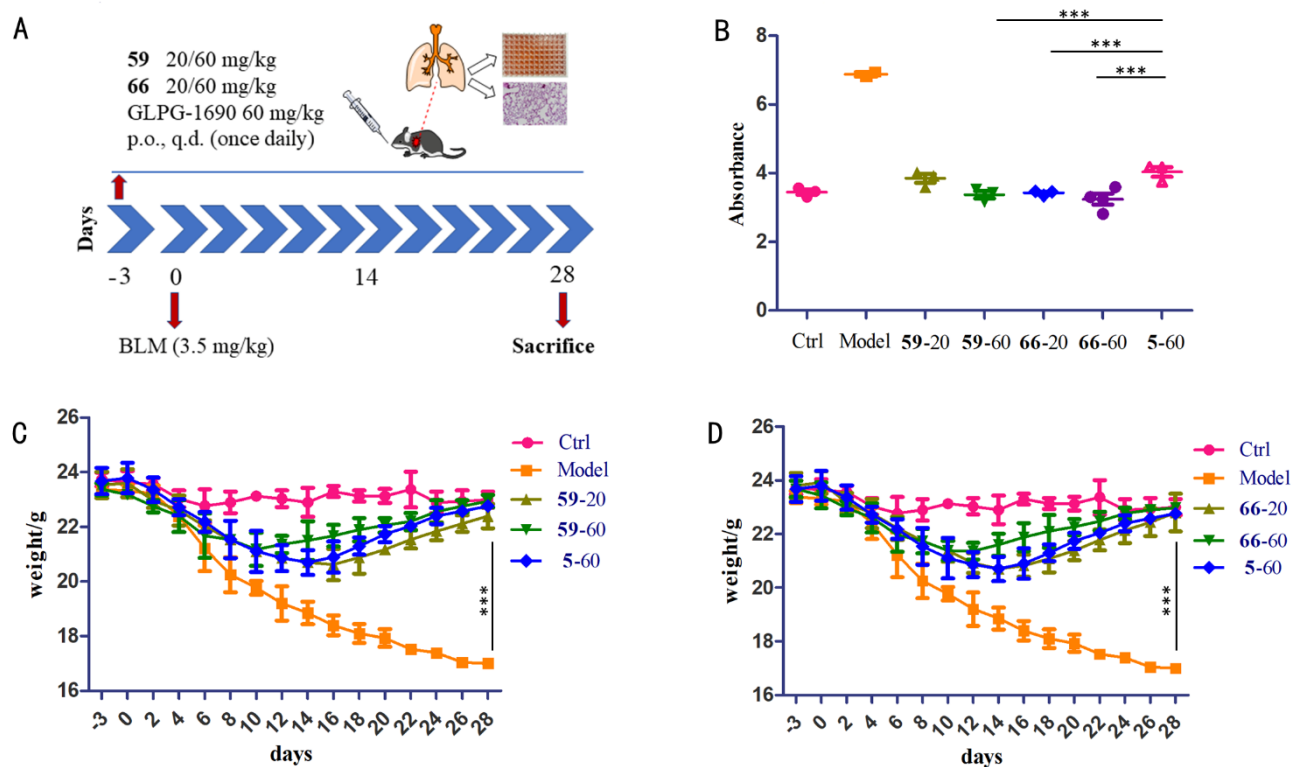


Figure 9. (A) Schematic representation of experimental protocol; (B) The *ex vivo* enzymatic assay of GLPG-1690 (**5**), **59** and **66** (data were drawn from the absorbance of the cleaved FS-3 by *in vivo* ATX; The tested lung homogenate samples were derived from the lung tissues in the BLM model treated with Trypsin); (C-D) Body weight change upon BLM administration under the effect of GLPG-1690, **59** and **66**. Values are presented as means (\pm SD); ***denotes statistical significance ($p < 0.05$, Mann-Whitney test).

It was of note that the model group presented a high ATX activity that was two folds over that in the control group (~ 7.09 vs ~ 3.45). In the groups under treatment with ATX inhibitors, there was obvious decrease in ATX activity. A consistency between the *in vitro* inhibition effect and *ex vivo* efficacy was observed for compounds **59** & **66** with GLPG-1690. **59** reduced the *ex vivo* ATX activity to a large degree (~ 3.85) and dose-dependent effect was present (~ 3.37 in 60 mg/kg). Alternatively, **66** exerted a better *ex vivo* efficacy than GLPG-1690 (~ 4.03 in 60 mg/kg) in both 20 (~ 3.43) and 60 mg/kg (~ 3.25), and a slightly dose-dependent effect was finally achieved. The promising *ex vivo* potency of **66** provided a rationale for the potential utilization in the animal models.

In vivo Effectiveness of 59 and 66 on a Bleomycin-induced Mice Pulmonary Fibrosis Model. The promising compounds **59** and **66** were tested for their efficacy in a 31-day model of pulmonary fibrosis induced by bleomycin. The severity of the lung tissues was evaluated by the modified Ashcroft score (grade 0~8) which further support the direct observation.^{36,37} The efficacy of inhibitors was evaluated based on histopathological changes in lung architecture through H&E staining (Figure 10) and Masson staining (Figure 11) inspection.³⁸ As shown in Figure 10A, bleomycin administration resulted in thickening of the alveolar septa, alveolar inflammation, and formation of fibrotic masses (6.28). ATX inhibition

by compounds **66**, **59** and GLPG-1690 generally improved lung texture: contiguous fibrotic walls and fewer fibrotic lesions were predominantly observed in microscopic field of H&E lung tissues. In the **59** group, the dose-dependent manner was much more obvious that the 20 mg/kg group present a high level of red staining (4.66). While in the 60 mg/kg group of **59**, similar biological effect (3.20) was observed with that in GLPG-1690 group (2.84).

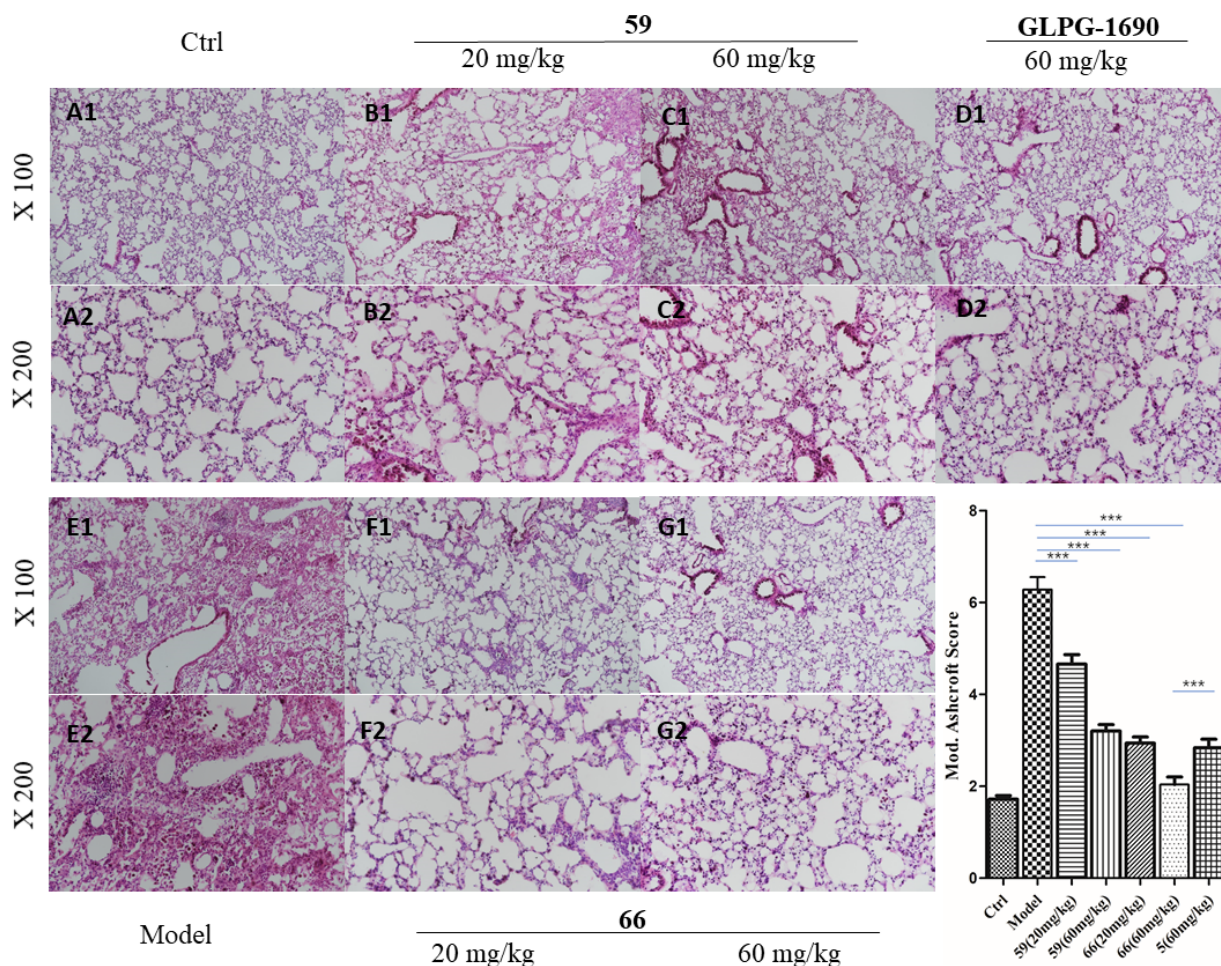


Figure 10. *In vivo* inhibition of ATX function with inhibitors alleviated BLM-induced pulmonary fibrosis viewing through H&E staining. (A) Representative stained sections from control mice; (B-C) BLM-challenged mice that received **59** in 20 or 60 mg/kg dose; (D) BLM-challenged mice that received GLPG-1690 in 60 mg/kg dose; (E) BLM-challenged mice that received vehicle as model group; (F-G) BLM-challenged mice that received **66** in 20 or 60 mg/kg dose; (A1-G1: $\times 100$ magnification, A2-G2: $\times 200$ magnification); (H) Quantitative histopathological analysis of fibrosis was performed by the modified Ashcroft score. Values are presented as means (\pm SD); ***denotes statistical significance ($p < 0.05$, Mann-Whitney test).

In the meantime, conform to the *in vivo* enzymatic assays, **66** displayed a better protection effect on the impaired lung architecture than **59**. In low doses (20 mg/kg), **66** could bring the BLM-exposed lung tissues to similar patterns with the control group. Amazingly, in high doses (60 mg/kg), **66** (2.04) exceeded the effect of GLPG-1690 (2.84) which suggested the potential application in fibrotic relevant diseases.

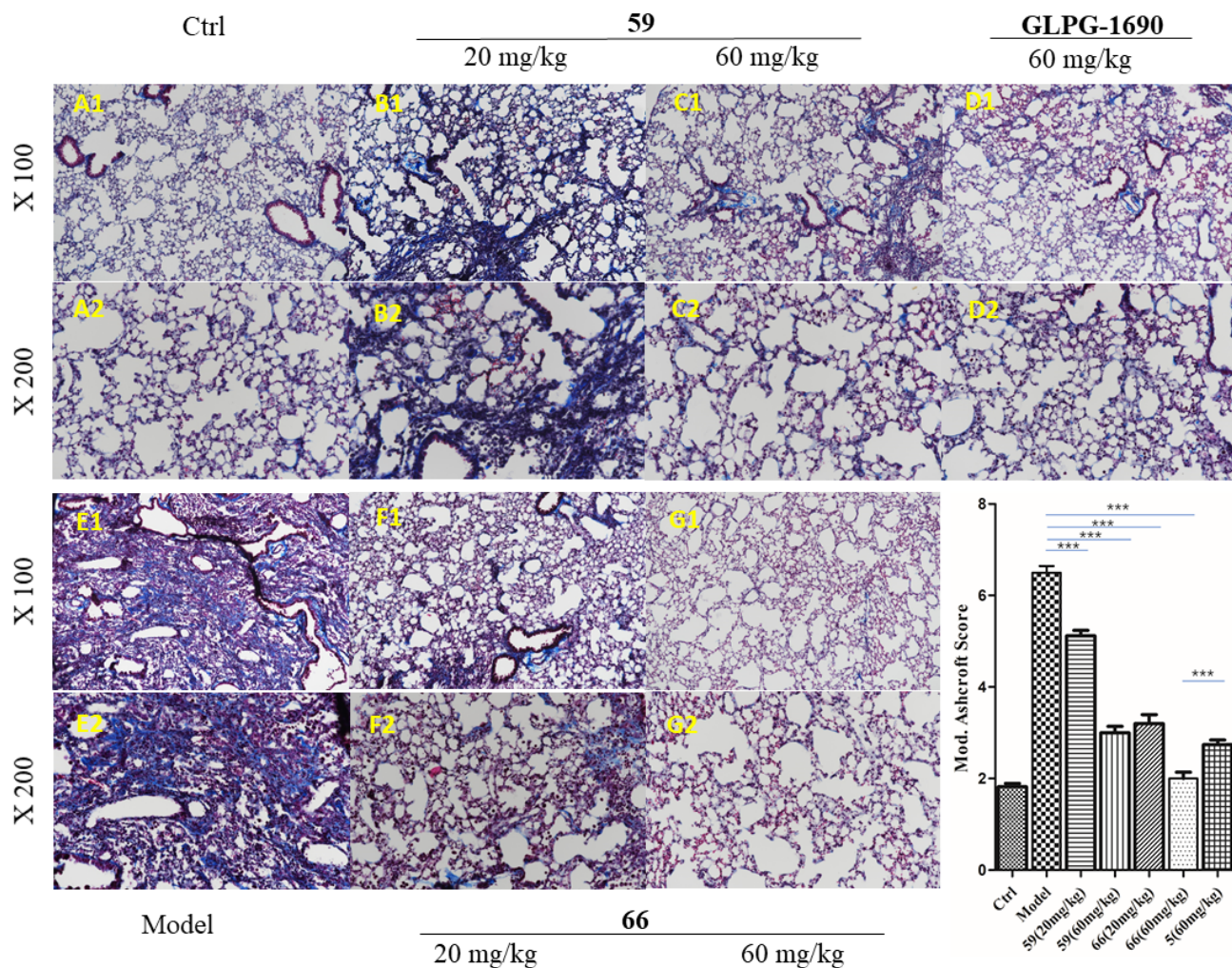


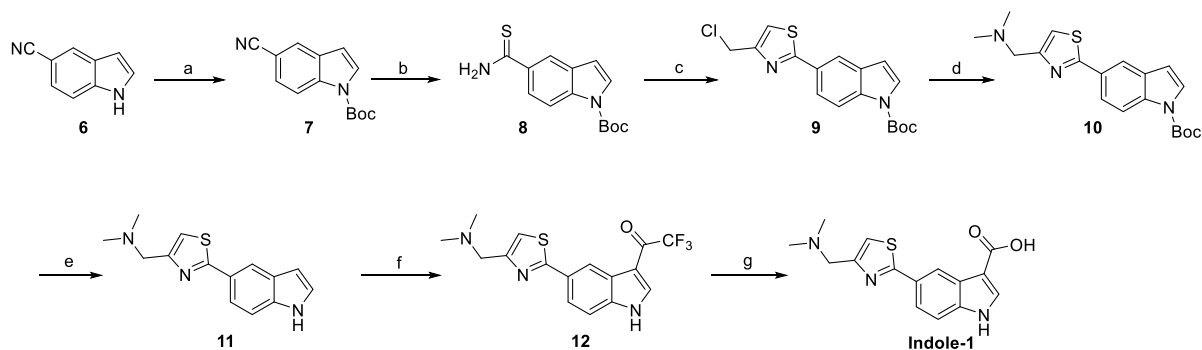
Figure 11. *In vivo* inhibition of ATX function with inhibitors alleviated BLM-induced pulmonary fibrosis viewing through Masson staining. (A) Representative stained sections from control mice; (B-C) BLM-challenged mice that received **59** in 20 or 60 mg/kg dose; (D) BLM-challenged mice that received GLPG-1690 in 60 mg/kg dose; (E) BLM-challenged mice that received vehicle as model group; (F-G) BLM-challenged mice that received **66** in 20 or 60 mg/kg dose; (A1-G1: $\times 100$, A2-G2: $\times 200$, magnification); (H) Quantitative histopathological analysis of fibrosis was performed by the modified Ashcroft score. Values are presented as means (\pm SD); ***denotes statistical significance ($p < 0.05$, Mann-Whitney test).

The Masson staining results of testing compounds were depicted in Figure 11. Generally, similar outcomes were harvested with the H&E staining assays. It was noteworthy that a significant difference was observed between the high doses of **66** (2.01) and GLPG-1690 (2.74). Although no superior results of **59** over GLPG-1690 were present in Masson staining assay, the repairing effects of **66** on the damaged lung texture deserved more attention.

Synthesis of indole-based allosteric ATX inhibitors. First of all, the lead compound **Indole-1** was synthesized as depicted in **Scheme 1**. The commercially available indole-5-carbonitrile (**6**) was reacted with di-tert-butyl-di-carbonate under 4-dimethylaminopyridine (DMAP) catalysis to obtain intermediate **7** in 94.3% yield. The cyano

group of **7** was conveniently converted to thioamide in the presence of sodium bisulfide and magnesium chloride hexahydrate to afford compound **8**.³⁹ Condensation of thioamide derivative (**8**) with 1,3-dichloropropan-2-one in toluene gave rise to **9**. Substitution of **9** with dimethylamine hydrochloride produced intermediate **10**, which was de-Boc by hydrochloric acid to resulted in **11**. Intermediate **11** was acylated using 2,2,2-trifluoroacetic anhydride in the presence of *N,N*-dimethyl formamide at 25 °C to afford **12** in 76.3% yield.⁴⁰ Finally, the trifluoroacetyl group in **12** was treated with 6 M NaOH at reflux to furnish **Indole-1**.⁴¹

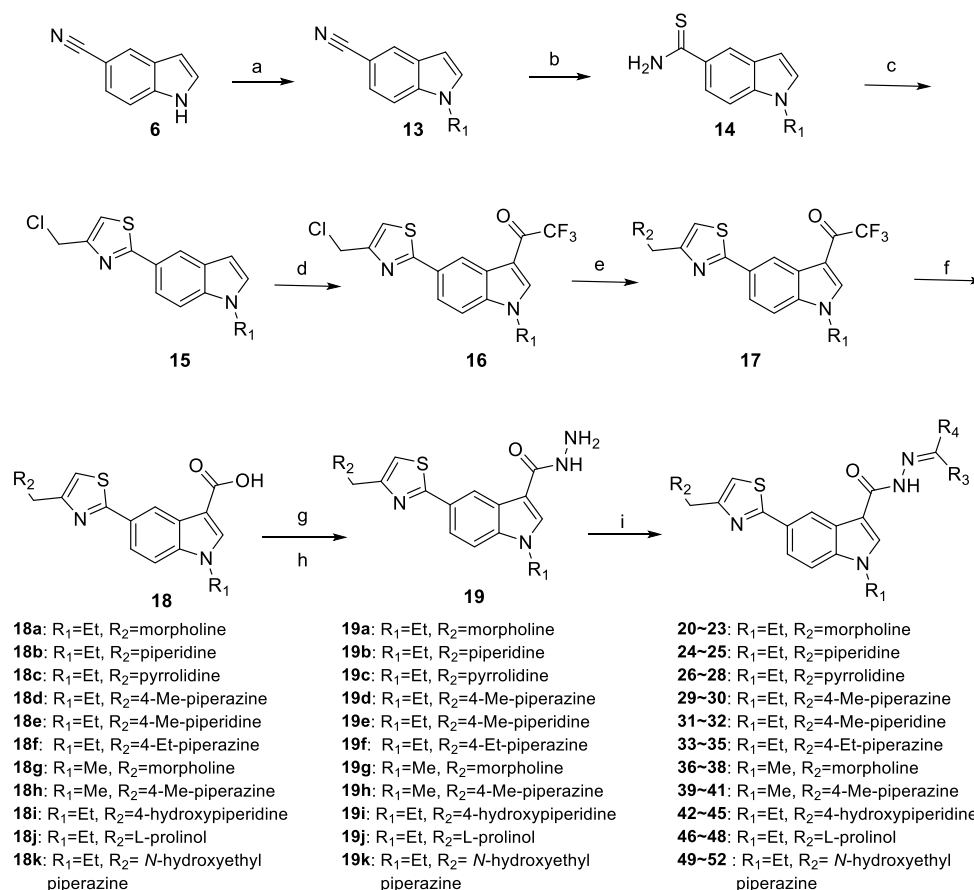
Scheme 1. Synthesis of Indole-1^a



^aReagents and conditions: (a) Boc₂O, DMAP, CH₂Cl₂, 25°C, 1 h; (b) NaHS, MgCl₂·6H₂O, DMF, 25 °C, 3 h; (c) 1,3-dichloropropan-2-one, toluene, reflux, 2.5 h; (d) dimethylamine·HCl, K₂CO₃, MeCN, 25 °C, 2 h; (e) 4 M HCl in MeOH, DCM, 25-50 °C, 6 h; (f) (CF₃CO)₂O, DMF, 55 °C, 2 h; (g) 6 N NaOH (aq.), MeOH, 70 °C, 2 h;

The synthetic efforts of acylhydrazone derivatives were outlined in Scheme 2. The starting material indole-5-carbonitrile **6** was utilized to undergo a typical *N*-alkylating (methylation or ethylation) reaction to obtain compound **13** in satisfying yields. Subsequently, the -CN group of **13** was treated with NaHS under the catalysis of MgCl₂·6H₂O to give the thioamide derivative **14** in 72.0% yield.³⁹ Next, a cyclization reaction took place between **14** and 1,3-dichloroacetone to furnish the thiazole species with a chloromethyl active site. Typically, a trifluoroacetylation reaction went ahead of the *N*-alkylation in the presence of trifluoroacetic anhydride in DMF to result in **16** in 78.1% yield with the chloromethyl unchanged.⁴⁰ Then, the *N*-alkylation between **16** and various amines were conducted in a K₂CO₃/MeCN system to bring **17a~17k** in 80.1~83.2% yields. Subsequently, the trifluoroacetyl group in **17a~17k** was hydrolyzed to corresponding -COOH derivatives **18a~18k** by treating with 6 M NaOH in reflux.⁴¹ **18a~18k** subjected to a sequential esterification and hydrazinolysis reaction gave rise to the acyl hydrazine species **19a~19k** as the products. Finally, **19a~19k** reacted with various aldehydes or ketones in ethanol to furnish the title compounds **20~52** in reasonable yields.

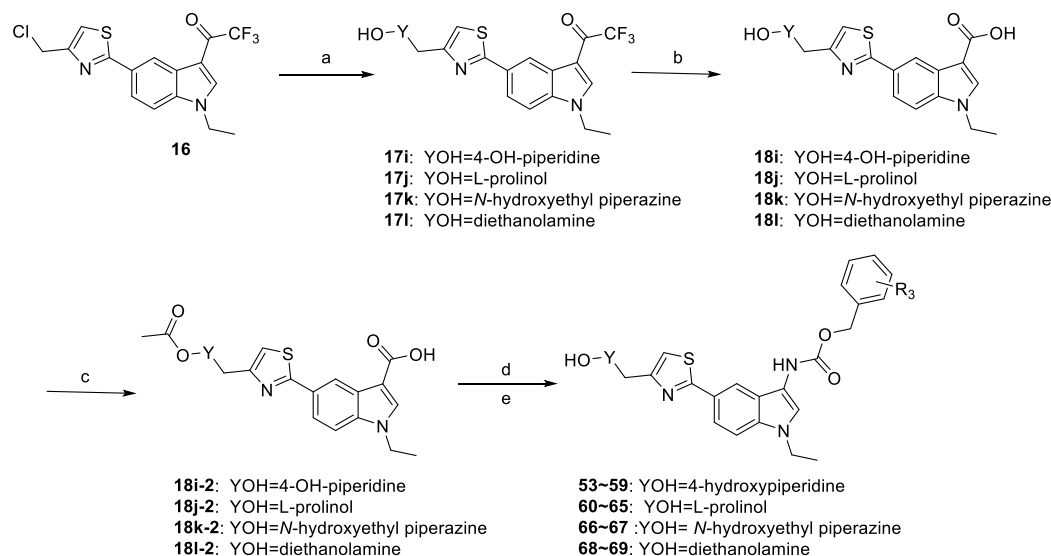
Scheme 2. Synthesis of compounds 20-52^a



^aReagents and conditions: (a) MeI or EtI, NaH, DMF, 25 °C, 1 h; (b) NaHS, MgCl₂·6H₂O, DMF, 25 °C, 3 h; (c) 1,3-dichloropropan-2-one, toluene, reflux, 2.5 h; (d) (CF₃CO)₂O, DMF, 0 °C to 25 °C, 1.5 h; (e) amine, K₂CO₃, MeCN, 25 °C, 2 h; (f) 6 N NaOH (aq.), 100 °C, 2 h; (g) MeOH, H₂SO₄, 25 °C-reflux, 2 h; (h) H₂N-NH₂·H₂O, EtOH, reflux, 2 h; (i) aldehyde or ketone, EtOH, reflux, 3 h.

Alternatively, the synthesis of the carbamate derivatives **53-69** was depicted in Scheme 3. **16** utilized as the starting material underwent a *N*-alkylation with secondary amines to give **17i-17l**, which was further transformed to the carboxylic acid counterpart **18** series. Subsequently, the -OH group containing amines in **18i-18l** were firstly undergoing a -OH protecting step using (CH₃CO)₂O as the acylating agent. The protected 3-indole carboxylic acid intermediates **18i-2-18l-2** were then rearranged to the carbamate derivatives followed by an ester hydrolysis reaction to furnish the final compounds **53-59**, **60-65**, **66-67** and **68-69**.⁴²

Scheme 3. Synthesis of compounds 53-69^a



^aReagents and conditions: (a) amines, K₂CO₃, MeCN, 25 °C, 2 h; (b) 6 N NaOH (aq.), 100 °C, 3 h; (c) (CH₃CO)₂O, CH₂Cl₂, 25 °C, 2 h; (d) DPPA, TEA, toluene, reflux, 2.5 h; (e) 1 N NaOH (aq.), dioxane, 25 °C, 2 h.

Conclusion

In conclusion, we report the optimization campaign from an indole-3-carboxylic acid lead **Indole-1** to the potent type IV ATX inhibitors **59** (1.01 nM) and **66** (0.43 nM) with IC₅₀ values even below 1 nM (GLPG-1690 1.3 nM). The SARs study showed that carbamate linker ideally bridged the indole skeleton and hydrophobic pocket binding aromatic group and brought an essential H-bond with residue Phe274 (the carbamate -NH in **66**). Meanwhile, the -OH containing amines well occupied the partial hydrophobic tunnel with the -OH in **66** made an extra H-bond with residue Gly256. In bleomycin induced mice pulmonary fibrosis model, compound **66** exerted better *ex vivo* ATX inhibiting effects with lower fluorescence absorbance (~3.25) than GLPG-1690 (~4.04) and a superior protection function on the injured lung tissues. Taken together, the identification of the carbamate-bearing indole based ATX inhibitors with preferred *in vitro* and *in vivo* potency may provide alternative therapy for fibrotic diseases.

Experimental

4.1 Chemistry

The melting points were obtained through a Büchi Melting Point B-540 facility (Büchi Labor technik, Flawil, Switzerland) which were uncorrected. Mass spectra (MS) were conducted in ESI mode on Agilent 1100 LC-MS (Agilent, Palo Alto, CA, USA) and a mixture of H₂O/MeCN (4:6) was utilized as the eluting system. The ¹H and ¹³C NMR spectra were performed by Bruker ARX-400 spectrometers (Bruker Bioscience, Billerica, MA, USA) using TMS as internal standard. Column chromatography was run on 200-300 mesh silica gel from Qingdao Ocean Chemicals (Qingdao, Shandong, China). Unless otherwise stated, all materials were commercially available and were used without further

1
2
3
4 purification. The purity of all target compounds was determined by HPLC analysis with a variable wavelength detector
5 (Agilent G1314F) that turned out to exceed 95% purity. The chromatography column was an Agilent column (ZORBAX
6 SB-C18, 5 μ m, 4.6 mm \times 150 mm, Agilent Corporation). Flow rate: 0.5 mL/min. Wavelength: 254 nm. Column temperature:
7 25 $^{\circ}$ C. Mobile phase: MeOH: H₂O = 95:5. The optical active compounds with one or two stereocenters were material-
8 derived and unchanged in the transforming procedures, so the optical rotation degrees were not given here.
9
10
11
12

13 **4.1.1 The synthetic procedures of the lead Indole-1**

14 **4.1.1.1 Synthesis of tert-butyl 5-cyano-1*H*-indole-1-carboxylate (7)**

15 Indole-5-carbonitrile (14.2 g, 0.1 mol) were introduced to a mixture of catalytic DMAP (0.25 g, 0.002 mol) in 80 mL
16 DCM and stirred for 10 min. Subsequently, di-tert-butyl di-carbonate (24.01 g, 0.11 mol) was added slowly and the system
17 was kept at ambient temperature for 1 h. Water (100 mL) was added to the mixture and the organic phase was separated,
18 concentrated to give white product **7** in 94.3% yield (22.82 g).
19
20
21
22
23
24

25 **4.1.1.2 Synthesis of tert-butyl 5-carbamothioyl-1*H*-indole-1-carboxylate (8)**

26 To a solvent of DMF (100 mL) was added NaHS (5.6 g, 0.1 mol), MgCl₂ \cdot 6H₂O (20.3 g, 0.1 mol) and **7** (12.1 g, 0.05
27 mol) under stirring. The reaction mixture was stirred at 25 $^{\circ}$ C for 3 h until completion. Water (500 mL) was added and the
28 mixture was filtered. The residue was transferred to 0.5 M HCl solution (200 mL), stirred for 20 min and filtered. The
29 resulting solid was washed with plenty of water to afford **8** as a yellow solid in 77.3% yield (10.68 g).
30
31
32
33
34

35 **4.1.1.3 Synthesis of tert-butyl 5-(4-(chloromethyl)thiazol-2-yl)-1*H*-indole-1-carboxylate (9)**

36 The 1,3-dichloropropan-2-one (1.92 g, 0.015 mol) and **8** (4.14 g, 0.015 mol) was dissolved in toluene (40 mL), stirred
37 at reflux for 2.5 h. When completed, the solvent was removed in vacuo and the residue was triturated with water. The
38 resulting precipitate was filtered, washed with water to give a yellow solid after drying in 81.3% yield (4.25 g).
39
40
41
42

43 **4.1.1.4 Synthesis of tert-butyl 5-(4-((dimethylamino)methyl)thiazol-2-yl)-1*H*-indole-1-carboxylate (10)**

44 Dimethylamine hydrochloride (0.2 mol) and K₂CO₃ (0.25 mol) were added to a stirred solution of **9** (3.48 g, 0.01 mol)
45 in MeCN (35 mL) at room temperature. After a 2 h stirring, the reaction mixture was filtered and the filtrate was evaporated.
46 The residue was taken up in water, stirred for 30 min, filtered to obtain yellow solid **10** in 75.3% yield (2.69 g).
47
48
49

50 **4.1.1.5 Synthesis of 1-(2-(1*H*-indol-5-yl)thiazol-4-yl)-*N,N*-dimethylmethanamine (11)**

51 **10** (2.51 g, 0.007 mol) was dissolved in DCM (10 mL) followed by slowly addition of 4 M HCl (g) in MeOH (20 mL).
52 The mixture was stirred at 50 $^{\circ}$ C for 6 h until the raw material was completely consumed. The solvent was removed in
53 vacuo followed by addition of water (100 mL). The aqueous portion was firstly extracted with DCM (40 mL) and the
54 organic layers were discarded. The pH of the aqueous phase was adjusted to 10 with 2 M NaOH and extracted with DCM
55 (60 mL \times 2). The organic layers were combined, dried over Na₂SO₄ and concentrated in vacuo to bring **11** in 69.3% yield
56
57
58
59
60

(1.25 g).

4.1.1.6 Synthesis of 1-(5-(4-((dimethylamino)methyl)thiazol-2-yl)-1*H*-indol-3-yl)-2,2,2-trifluoroethan-1-one (**12**)

At room temperature, **11** (1.03 g, 0.004 mol) was dissolved in DMF (20 mL). 2,2,2-trifluoroacetic anhydride (0.6 mol) was added dropwise at 0°C. After addition, the reaction mixture was stirred at 55°C for 2 h. When the reaction is completed as indicated by the TLC result, the mixture was poured into water (80 mL) and stirred for 30 min. The solution was filtered to give **12** as a brown solid in 76.3% yield (1.08 g).

4.1.1.7 Synthesis of 5-(4-((dimethylamino)methyl)thiazol-2-yl)-1*H*-indole-3-carboxylic acid (**Indole-1**)

Intermediate **12** (0.71 g, 0.002 mol) were added to a mixed solvent of 10 mL 4 M aqueous NaOH and 3 mL MeOH which was refluxed for 2 h. The reaction mixture was cooled to room temperature and the MeOH was purged followed by addition of more water (20 mL). The aqueous solution was extracted with *n*-BuOH (20 mL), dried over Na₂SO₄, and the organic layer was concentrated to give the crude product to be involved in column chromatography purification with an eluting system of DCM: MeOH: HOAc=20:1:1 to furnish **Indole-1** in 57.2% yield (0.35 g). ¹H NMR (400 MHz, DMSO) δ 12.09 (s, 1H), 8.66 (s, 1H), 8.05 (s, 1H), 7.76 (d, *J* = 8.4 Hz, 1H), 7.55 (d, *J* = 8.5 Hz, 1H), 7.38 (s, 1H), 4.64 (s, 2H). ¹³C NMR (101 MHz, DMSO) δ 168.92, 159.18, 137.93, 133.75, 126.93, 126.90, 121.06, 119.17, 114.04, 113.29, 109.68, 60.33. The dimethylamine signals (RN(CH₃)₂) in both ¹H and ¹³C spectrum were both sheltered by the DMSO solvent signal which were not apparently shown.

4.1.2 The synthetic procedures and structural determination of all target compounds were present as following.

4.1.3 1-ethyl-1*H*-indole-5-carbonitrile (**13**)

60% NaH (200.2 g, 5.0 mol) was suspended in DMF (800 mL) at ambient temperature. 1*H*-indole-5-carbonitrile (284.0 g, 2.0 mol) was added when the temperature reached to 40 °C. After the gas escaped, the solution was cooled to 25°C. Then iodoethane (468.0 g, 3.0 mol) was added and the reaction mixture was stirred at room temperature for 2 h. When completed, the mixture was diluted with water (1500 mL). After stirring for 0.5 h, the mixture was filtered to obtain the solid **13** in 88% yield.

4.1.4 1-ethyl-1*H*-indole-5-carbothioamide (**14**)

To a solvent of DMF (600 mL) was added NaHS (85.0 g, 3.5 mol), MgCl₂·6H₂O (406.0 g, 2 mol) and **13** (170 g, 0.7 mol) under stirring. The reaction mixture was stirred at 25°C for 3 h until completion. After cooling to room temperature, water was added, filtered. The residue was transferred to 1 M HCl solution (600 mL) and stirred for 20 min and filtered. The resulting solid was washed with plenty of water to afford the title compound **14** as a yellow solid in 72.1% yield. ¹H NMR (600 MHz, DMSO) δ 9.58 (s, 1H), 9.33 (s, 1H), 8.25 (d, *J* = 1.6 Hz, 1H), 7.84 (dd, *J* = 8.7, 1.8 Hz, 1H), 7.48 (d, *J* = 2.0 Hz, 1H), 7.47 (d, *J* = 3.5 Hz, 1H), 6.56 – 6.54 (m, 1H), 4.23 (q, *J* = 7.2 Hz, 2H), 1.35 (t, *J* = 7.2 Hz, 3H).

4.1.5 4-(chloromethyl)-2-(1-ethyl-1*H*-indol-5-yl)thiazole (**15**)

At room temperature, the 1,3-dichloropropan-2-one (63 g, 0.5 mol) and **14** (102 g, 0.5 mol) was dissolved in toluene (600 mL), stirring at reflux for 2.5 h. When completed, the solvent was removed in vacuo and the residue was triturated with water. The resulting precipitate was filtered, washed with water to give a yellow solid after drying in 78.9% yield. ¹H NMR (600 MHz, DMSO) δ 8.17 (d, *J* = 1.5 Hz, 1H), 7.74 (dd, *J* = 8.6, 1.7 Hz, 1H), 7.69 (s, 1H), 7.59 (d, *J* = 8.6 Hz, 1H), 7.49 (d, *J* = 3.1 Hz, 1H), 6.58–6.57 (m, 1H), 4.87 (s, 2H), 4.24 (q, *J* = 7.2 Hz, 2H), 1.38 (t, *J* = 7.2 Hz, 3H).

4.1.6 1-(5-(4-(chloromethyl)thiazol-2-yl)-1-ethyl-1*H*-indol-3-yl)-2,2,2-trifluoroethan-1-one(**16**)

At room temperature, **15** (108 g, 0.4 mol) was dissolved in DMF (800 mL). 2,2,2-trifluoroacetic anhydride (0.6 mol) was added dropwise at 0°C. After addition, the reaction mixture was stirred at ambient temperature for 1.5 h. When the reaction is completed as indicated by the TLC result, the mixture was poured into water (2500 mL) and stirred for 30 min. The solution was filtered to give **16** as a solid 113.5 g in 78.1% yield. ¹H NMR (600 MHz, DMSO) δ 8.80 (d, *J* = 1.4 Hz, 1H), 8.70 (d, *J* = 1.6 Hz, 1H), 7.98 (dd, *J* = 8.6, 1.8 Hz, 1H), 7.88 (d, *J* = 8.7 Hz, 1H), 7.82 (s, 1H), 4.93 (s, 2H), 4.45 (q, *J* = 7.2 Hz, 2H), 1.46 (t, *J* = 7.2 Hz, 3H). ¹³C NMR (101 MHz, DMSO) δ 168.60, 153.30, 141.29, 137.88, 129.17, 127.27, 123.28, 119.66, 119.54, 118.63, 115.73, 113.08, 108.81, 42.62, 41.44, 15.61. MS (ESI) *m/z* (%): 373.37 [(*M*+*H*)⁺, 100].

4.1.7 General procedure for preparation of intermediate **17** (**17a-17l**)

Amine (0.2 mol) and K₂CO₃ (0.25 mol) were added to a stirred solution of **16** (0.1mol) in MeCN (350 mL) at room temperature. After a 2 h stirring, the reaction mixture was filtered and the filtrate was evaporated. The residue was taken up in water, stirred for 30 min, filtered to give orange solids **17a-17l** in 80.1% to 83% yield.

1-(1-ethyl-5-(4-((4-hydroxypiperidin-1-yl)methyl)thiazol-2-yl)-1*H*-indol-3-yl)-2,2,2-trifluoroethan-1-one(**17i**): ¹H NMR (600 MHz, DMSO) δ 8.78 (d, *J* = 1.5 Hz, 1H), 8.69 (d, *J* = 1.6 Hz, 1H), 7.97 (dd, *J* = 8.6, 1.7 Hz, 1H), 7.86 (d, *J* = 8.7 Hz, 1H), 7.47 (s, 1H), 4.56 (d, *J* = 3.9 Hz, 1H), 4.45 (q, *J* = 7.2 Hz, 2H), 3.64 (s, 2H), 3.46 (d, *J* = 3.7 Hz, 1H), 2.79 (d, *J* = 10.5 Hz, 2H), 2.16 (s, 2H), 1.73 (d, *J* = 9.5 Hz, 2H), 1.46 (t, *J* = 7.2 Hz, 3H), 1.44–1.39 (m, 2H).

(*S*)-1-(1-ethyl-5-(4-((2-(hydroxymethyl)pyrrolidin-1-yl)methyl)thiazol-2-yl)-1*H*-indol-3-yl)-2,2,2-trifluoroethan-1-one (**17j**): ¹H NMR (600 MHz, DMSO) δ 8.78 (d, *J* = 1.6 Hz, 1H), 8.69 (d, *J* = 1.6 Hz, 1H), 7.97 (dd, *J* = 8.6, 1.7 Hz, 1H), 7.86 (d, *J* = 8.6 Hz, 1H), 7.48 (s, 1H), 4.45 (q, *J* = 7.2 Hz, 2H), 4.15 (d, *J* = 14.3 Hz, 1H), 3.72 (d, *J* = 14.3 Hz, 1H), 3.47 (dd, *J* = 10.5, 4.4 Hz, 1H), 3.32 (dd, *J* = 10.5, 6.5 Hz, 1H), 3.03 (dt, *J* = 9.3, 4.6 Hz, 1H), 2.74–2.66 (m, 1H), 2.39 (q, *J* = 8.5 Hz, 1H), 1.84 (dq, *J* = 12.2, 8.2 Hz, 1H), 1.70–1.61 (m, 2H), 1.58 (dt, *J* = 19.3, 6.5 Hz, 1H), 1.46 (t, *J* = 7.3 Hz, 3H). ¹³C NMR (101 MHz, DMSO) δ 167.16, 156.57, 141.13, 137.67, 129.72, 127.27, 123.23, 119.40, 118.65, 116.48, 115.75, 112.97, 108.78, 64.98, 64.58, 54.60, 54.50, 42.60, 28.45, 23.14, 15.61.

4.1.8 General procedure for preparation of intermediate **18** (**18a-18l**)

Intermediates **17a-17l** (0.08 mol) were added to 120 mL 4 M aqueous NaOH and refluxed for 2 h. The reaction mixture was cooled to room temperature and the products **18a-18l** were obtained in quantitative yield through a principle filtration in reduced pressure.

4.1.9 General procedure for preparation of intermediate **19** (**19a-19l**)

Intermediates **18a-18l** (0.05 mol) were dissolved in 200 mL MeOH followed by slowly addition of concentrated H₂SO₄ (5 mL). The mixture was refluxed for 2-5 h until the completely consumption of the raw materials. The solvent was removed in reduced pressure, 200 mL water was introduced and the mixture was extracted with EA (150 mL × 2). The organic layers were combined, dried with anhydrous Na₂SO₄, and concentrated in vacuum to give oil materials which were used in the following step without further purification.

The oil materials obtained (0.02 mol) and 15 mL hydrazine hydrate were dissolved in 150 mL EtOH and the system was refluxed for 2.5 h. After completion, the solvent was discarded in vacuum followed by extraction with DCM in water. The organic phase was concentrated to give a raw material which was further purified in column chromatography (DCM: MeOH= 30~10:1) to give **19a-19l** as yellow solids in reasonable yields (40% ~70%).

4.1.10 General procedure for preparation of target compounds **20-52**

Intermediates **19a-19k** (1 mmol) and aldehydes/ketones (1.2 mmol) were added to 15 mL EtOH and refluxed for 3 h. For **20~23**, the final product precipitated from the solvent which could be accessed through direct filtration with high purities. For compounds **24~52**, the solvents were purged to give the crude products which were further purified with column chromatography/*p*-TLC (DCM: MeOH= 40~15:1) in acceptable yields.

(*E*)-1-ethyl-*N'*-(4-fluorobenzylidene)-5-(4-(morpholinomethyl)thiazol-2-yl)-1*H*-indole-3-carbohydrazide (**20**). mp 212-214 °C. ¹H NMR (400 MHz, CDCl₃) δ 8.87 (s, 1H), 8.44 (s, 1H), 7.84 (s, 1H), 7.59 (s, 2H), 7.33 (s, 1H), 7.29 (s, 2H), 6.98 (s, 2H), 4.15 (s, 2H), 3.95 (s, 2H), 3.86 (s, 4H), 2.85 (s, 4H), 1.48 (s, 3H). ¹³C NMR (101 MHz, CDCl₃) δ 169.81, 164.89, 162.40, 136.88, 134.40, 132.29, 130.64, 130.61, 129.01, 128.93, 127.37, 121.55, 121.00, 120.86, 118.10, 117.91, 115.94, 115.72, 110.15, 65.88, 57.69, 52.96(2C), 41.81, 29.71, 15.11. MS (ESI) *m/z* (%): 492.24 [(M+H)⁺,65].

(*E*)-1-ethyl-*N'*-(4-methoxybenzylidene)-5-(4-(morpholinomethyl)thiazol-2-yl)-1*H*-indole-3-carbohydrazide (**21**). mp 222-224 °C. ¹H NMR (400 MHz, DMSO) δ 11.45 (s, 1H), 8.85 (s, 1H), 8.33 (s, 1H), 7.84 (d, *J* = 8.2 Hz, 1H), 7.70 (s, 2H), 7.68 (s, 1H), 7.45 (s, 1H), 7.04 (d, *J* = 7.9 Hz, 2H), 4.35 (s, 2H), 3.82 (s, 3H), 3.66 (s, 2H), 3.61 (s, 3H), 2.51 (s, 3H), 1.47 (t, *J* = 6.6 Hz, 3H). ¹³C NMR (101 MHz, DMSO) δ 168.46, 160.98, 154.32, 132.27, 130.44, 128.85(2C), 127.70, 127.13, 124.28, 121.24, 119.97, 118.18, 116.64, 116.01, 114.83(2C), 111.60, 109.14, 66.65(2C), 58.46, 55.75, 53.65(2C), 41.62, 15.64. MS (ESI) *m/z* (%): 504.23 [(M+H)⁺,55].

(*E*)-*N'*-(benzo[*d*][1,3]dioxol-5-ylmethylene)-1-ethyl-5-(4-(morpholinomethyl)thiazol-2-yl)-1*H*-indole-3-carbohydrazide

1
2
3
4 (22). mp 208-210 °C. ¹H NMR (400 MHz, DMSO) δ 11.47 (s, 1H), 8.85 (s, 1H), 8.31 (s, 2H), 7.83 (s, 1H), 7.69 (s, 1H),
5
6 7.44 (s, 1H), 7.33 (s, 1H), 7.16 (s, 1H), 7.01 (s, 1H), 6.11 (s, 2H), 4.34 (s, 2H), 3.65 (s, 2H), 3.61 (s, 4H), 2.49 (m, 4H),
7
8 1.47 (t, *J* = 7.2 Hz, 3H). ¹³C NMR (101 MHz, DMSO) δ 168.45, 161.16, 154.33, 149.20, 148.48, 129.57, 128.78, 127.16,
9
10 125.58, 123.37, 121.24, 120.03, 116.62, 111.58, 109.03, 108.94, 106.45, 105.46, 102.18, 101.95, 66.65(2C), 58.46,
11
12 53.65(2C), 41.60, 15.60. MS (ESI) *m/z* (%): 518.18 [(M+H)⁺, 45].

13
14 (*E*)-1-ethyl-*N'*-(1-(4-fluorophenyl)ethylidene)-5-(4-(morpholinomethyl)thiazol-2-yl)-1*H*-indole-3-carbohydrazide (23).
15
16 mp 211-213 °C. ¹H NMR (400 MHz, DMSO) δ 10.41 (s, 1H), 8.84 (s, 1H), 8.43 (s, 1H), 7.93 – 7.87 (m, 2H), 7.84 (d, *J* =
17
18 8.5 Hz, 1H), 7.70 (d, *J* = 8.6 Hz, 1H), 7.45 (s, 1H), 7.28 (t, *J* = 8.7 Hz, 2H), 4.33 (q, *J* = 7.1 Hz, 2H), 3.66 (s, 2H), 3.61 (s,
19
20 4H), 2.49 (s, 3H), 2.39 (s, 3H), 1.46 (t, *J* = 7.2 Hz, 3H). ¹³C NMR (101 MHz, DMSO) δ 168.47, 164.36, 161.91, 154.37,
21
22 136.94, 135.56, 135.54, 128.89(2C), 128.80, 128.22, 127.16, 121.22, 120.05, 116.61, 115.84(2C), 115.63, 111.58, 108.76,
23
24 66.67(2C), 58.46, 53.65(2C), 41.60, 15.60, 14.44. MS (ESI) *m/z* (%): 506.20 [(M+H)⁺, 100].

25
26 (*E*)-1-ethyl-*N'*-(4-fluorobenzylidene)-5-(4-(piperidin-1-ylmethyl)thiazol-2-yl)-1*H*-indole-3-carbohydrazide (24). mp 201-
27
28 203 °C. ¹H NMR (400 MHz, DMSO) δ 11.60 (s, 1H), 8.84 (s, 1H), 8.42 (s, 1H), 7.84 (dd, *J* = 8.6, 1.5 Hz, 1H), 7.80 (dd, *J*
29
30 = 8.5, 5.7 Hz, 2H), 7.70 (d, *J* = 8.6 Hz, 1H), 7.43 (s, 1H), 7.31 (t, *J* = 8.8 Hz, 2H), 4.35 (d, *J* = 6.3 Hz, 2H), 3.68 (s, 2H),
31
32 3.38 (s, 4H), 1.54 (d, *J* = 5.1 Hz, 3H), 1.47 (t, *J* = 7.2 Hz, 3H), 1.40 (d, *J* = 4.3 Hz, 2H). ¹³C NMR (101 MHz, DMSO) δ
33
34 159.55, 159.12, 155.78, 155.10, 152.27, 138.67, 138.57, 135.34, 131.90, 131.33, 129.28, 124.93, 123.89, 123.55, 123.37,
35
36 122.43, 108.86, 104.49, 101.85, 55.88, 55.40, 45.99, 45.23, 37.00, 29.45, 15.32, 8.93. MS (ESI) *m/z* (%): 490.17 [(M+H)⁺,
37
38 100].

39
40 (*E*)-*N'*-(benzo[*d*][1,3]dioxol-5-ylmethylene)-1-ethyl-5-(4-(piperidin-1-ylmethyl)thiazol-2-yl)-1*H*-indole-3-
41
42 carbohydrazide (25). mp 196-198 °C. ¹H NMR (400 MHz, DMSO) δ 11.56 (s, 1H), 8.84 (s, 1H), 8.38 (s, 2H), 7.84 (d, *J* =
43
44 8.6 Hz, 1H), 7.70 (d, *J* = 8.7 Hz, 1H), 7.44 (s, 1H), 7.33 (s, 1H), 7.16 (d, *J* = 7.8 Hz, 1H), 7.01 (d, *J* = 8.0 Hz, 1H), 6.11 (s,
45
46 2H), 4.34 (s, 2H), 3.68 (s, 2H), 1.55 (s, 4H), 1.47 (t, *J* = 7.2 Hz, 3H), 1.40 (s, 2H). ¹³C NMR (101 MHz, DMSO) δ 168.40,
47
48 160.66, 154.44, 149.20, 148.48, 145.42, 143.09, 137.17, 132.26, 129.59, 127.98, 127.15, 123.37, 121.24, 120.02, 116.74,
49
50 111.61, 108.96, 105.45, 101.95, 58.59, 54.26, 41.60, 25.74, 24.19, 15.62. MS (ESI) *m/z* (%): 516.70 [(M+H)⁺, 100].

51
52 (*E*)-1-ethyl-*N'*-(4-methoxybenzylidene)-5-(4-(pyrrolidin-1-ylmethyl)thiazol-2-yl)-1*H*-indole-3-carbohydrazide (26).
53
54 mp 182-184 °C. ¹H NMR (400 MHz, DMSO) δ 11.55 (s, 1H), 8.87 (s, 1H), 8.36 (s, 2H), 7.86 (d, *J* = 8.7 Hz, 1H), 7.72 (d,
55
56 *J* = 8.6 Hz, 1H), 7.64 (s, 1H), 7.62 (s, 2H), 7.29 (d, *J* = 7.9 Hz, 2H), 4.35 (s, 2H), 4.12 (s, 1H), 2.93 (s, 3H), 2.36 (s, 3H),
57
58 1.83 (s, 3H), 1.48 (t, *J* = 7.1 Hz, 3H). ¹³C NMR (101 MHz, DMSO) δ 162.76, 159.02, 157.52, 155.78, 155.11, 152.20,
59
60 138.63, 138.15, 135.33, 131.34, 124.81, 123.95, 123.61, 123.43, 122.83, 119.81, 108.85, 104.57, 101.80, 55.89, 55.37,
42.76, 41.58, 40.29, 36.24, 31.22, 15.31. MS (ESI) *m/z* (%): 488.15 [(M+H)⁺, 100].

1
2
3
4 (*E*)-*N'*-(4-chlorobenzylidene)-1-ethyl-5-(4-(pyrrolidin-1-ylmethyl)thiazol-2-yl)-1*H*-indole-3-carbohydrazide (**27**). mp
5 193-195 °C. ¹H NMR (400 MHz, DMSO) δ 11.81 (s, 1H), 8.88 (s, 1H), 8.49 (s, 1H), 7.83 (d, *J* = 8.4 Hz, 1H), 7.75 (d, *J* =
6 8.2 Hz, 2H), 7.67 (d, *J* = 8.6 Hz, 1H), 7.51 (d, *J* = 8.2 Hz, 2H), 7.47 (s, 1H), 4.32 (d, *J* = 4.4 Hz, 3H), 3.86 (d, *J* = 21.1 Hz,
7 2H), 2.69 (s, 5H), 1.74 (s, 5H), 1.46 (t, *J* = 7.1 Hz, 4H). ¹³C NMR (101 MHz, DMSO) δ 168.55, 164.55, 161.10, 154.38,
8 137.08, 134.46, 134.14, 129.37(2C), 128.87(2C), 128.67, 127.17, 121.31, 120.03, 116.72, 111.61, 110.11, 108.85, 55.09,
9 53.89(2C), 41.64, 23.58(2C), 15.58. MS (ESI) *m/z* (%): 492.38 [(*M*+*H*)⁺, 100].

10
11
12
13
14
15 (*E*)-1-ethyl-*N'*-(1-(4-fluorophenyl)ethylidene)-5-(4-(pyrrolidin-1-ylmethyl)thiazol-2-yl)-1*H*-indole-3-carbohydrazide (**28**).
16 mp 194-196 °C. ¹H NMR (400 MHz, DMSO) δ 10.41 (s, 1H), 8.84 (s, 1H), 8.44 (s, 1H), 7.89 (dd, *J* = 8.3, 5.8 Hz, 2H),
17 7.85 (dd, *J* = 8.7, 1.5 Hz, 1H), 7.71 (d, *J* = 8.7 Hz, 1H), 7.51 (s, 1H), 7.29 (t, *J* = 8.8 Hz, 2H), 4.33 (q, *J* = 7.2 Hz, 2H), 3.93
18 (s, 2H), 2.73 (s, 4H), 2.39 (s, 3H), 1.77 (s, 4H), 1.46 (t, *J* = 7.2 Hz, 3H). MS (ESI) *m/z* (%): 490.17 [(*M*+*H*)⁺, 100].

19
20
21
22
23 (*E*)-1-ethyl-*N'*-(1-(4-fluorophenyl)ethylidene)-5-(4-((4-methylpiperazin-1-yl)methyl)thiazol-2-yl)-1*H*-indole-3-
24 carbohydrazide (**29**). mp 213-215 °C. ¹H NMR (400 MHz, DMSO) δ 10.41 (s, 1H), 8.82 (s, 1H), 8.44 (s, 1H), 7.89 (s, 2H),
25 7.83 (s, 1H), 7.71 (s, 1H), 7.42 (s, 1H), 7.29 (s, 2H), 4.32 (s, 2H), 3.65 (s, 2H), 2.39 (m, 8H), 2.17 (s, 3H), 1.46 (t, *J* = 7.1
26 Hz, 3H), 1.23 (s, 3H). MS (ESI) *m/z* (%): 519.70 [(*M*+*H*)⁺, 100].

27
28
29
30
31 (*E*)-*N'*-(benzo[*d*][1,3]dioxol-5-ylmethylene)-1-ethyl-5-(4-((4-methylpiperazin-1-yl)methyl)thiazol-2-yl)-1*H*-indole-3-
32 carbohydrazide (**30**). mp 204-206 °C. ¹H NMR (400 MHz, DMSO) δ 11.44 (s, 1H), 8.84 (s, 1H), 8.32 (s, 2H), 7.83 (s, 1H),
33 7.71 (s, 1H), 7.39 (s, 1H), 7.33 (s, 1H), 7.18 (s, 1H), 7.02 (s, 1H), 6.11 (s, 2H), 4.35 (s, 2H), 3.62 (s, 2H), 2.51 (s, 4H), 2.46
34 (s, 4H), 1.52 (s, 3H), 1.49 (t, *J* = 7.1 Hz, 3H). ¹³C NMR (101 MHz, DMSO) δ 168.23, 160.92, 155.19, 149.20, 148.48,
35 145.39, 137.02, 129.58, 127.23, 123.35, 121.23, 120.02, 116.11, 113.66, 111.58, 108.95, 108.43, 105.48, 104.43, 101.94,
36 58.98, 54.43(2C), 41.60, 26.03(2C), 24.43, 15.61. MS (ESI) *m/z* (%): 531.27 [(*M*+*H*)⁺, 100].

37
38
39
40
41
42 (*E*)-1-ethyl-*N'*-(4-fluorobenzylidene)-5-(4-((4-methylpiperidin-1-yl)methyl)thiazol-2-yl)-1*H*-indole-3-carbohydrazide
43 (**31**). mp 210-212 °C. ¹H NMR (400 MHz, DMSO) δ 11.63 (s, 1H), 8.86 (s, 1H), 8.44 (s, 2H), 7.85 (dd, *J* = 8.7, 1.4 Hz,
44 1H), 7.80 (dd, *J* = 8.6, 5.7 Hz, 2H), 7.71 (d, *J* = 8.6 Hz, 1H), 7.52 (s, 1H), 7.32 (t, *J* = 7.2 Hz, 2H), 4.35 (d, *J* = 6.6 Hz, 2H),
45 3.83 (s, 2H), 3.03 (d, *J* = 11.0 Hz, 2H), 2.27 (s, 2H), 1.64 (d, *J* = 12.0 Hz, 2H), 1.47 (t, *J* = 7.2 Hz, 3H), 1.40 (m, 1H) 1.24
46 (d, *J* = 11.0 Hz, 2H), 0.90 (d, *J* = 6.4 Hz, 3H). ¹³C NMR (101 MHz, DMSO) δ 168.69, 164.55, 162.10, 154.64, 153.10,
47 132.58, 132.49, 131.76, 129.44, 129.36, 127.10, 121.34, 120.10, 117.74, 116.47, 116.25, 116.12, 115.90, 111.67, 57.53,
48 53.36, 41.66, 33.51, 30.10, 22.03, 15.62. MS (ESI) *m/z* (%): 504.60 [(*M*+*H*)⁺, 100].

49
50
51
52
53
54 (*E*)-*N'*-(benzo[*d*][1,3]dioxol-5-ylmethylene)-1-ethyl-5-(4-((4-methylpiperidin-1-yl)methyl)thiazol-2-yl)-1*H*-indole-3-
55 carbohydrazide (**32**). mp 210-212 °C. ¹H NMR (400 MHz, DMSO) δ 11.42 (s, 1H), 8.83 (s, 1H), 8.31 (s, 2H), 7.83 (d, *J* =
56 8.2 Hz, 1H), 7.69 (d, *J* = 8.6 Hz, 1H), 7.38 (s, 1H), 7.33 (s, 1H), 7.17 (d, *J* = 7.8 Hz, 1H), 7.00 (d, *J* = 8.0 Hz, 1H), 6.10 (s,
57
58
59
60

2H), 4.34 (d, $J = 5.7$ Hz, 2H), 3.62 (s, 2H), 2.90 (d, $J = 10.8$ Hz, 2H), 2.02 (t, $J = 11.0$ Hz, 2H), 1.58 (d, $J = 11.7$ Hz, 2H), 1.47 (t, $J = 7.1$ Hz, 3H), 1.32 (s, 1H), 1.17 (dd, $J = 22.0, 10.2$ Hz, 2H), 0.89 (d, $J = 6.3$ Hz, 3H). MS (ESI) m/z (%): 530.59 [(M+H)⁺, 45].

(*E*)-1-ethyl-5-(4-((4-ethylpiperazin-1-yl)methyl)thiazol-2-yl)-*N'*-(4-fluorobenzylidene)-1*H*-indole-3-carbohydrazide (**33**). mp 170-172 °C. ¹H NMR (400 MHz, DMSO) δ 11.57 (s, 1H), 8.84 (s, 1H), 8.39 (s, 2H), 7.84 (dd, $J = 8.7, 1.7$ Hz, 1H), 7.80 (dd, $J = 8.7, 5.6$ Hz, 2H), 7.70 (d, $J = 8.6$ Hz, 1H), 7.41 (s, 1H), 7.31 (t, $J = 8.8$ Hz, 2H), 4.35 (q, $J = 6.8$ Hz, 2H), 3.65 (s, 2H), 2.41 (m, 6H), 2.32 (dd, $J = 14.3, 7.2$ Hz, 4H), 1.47 (t, $J = 7.2$ Hz, 3H), 0.98 (t, $J = 7.2$ Hz, 3H). ¹³C NMR (101 MHz, DMSO) δ 168.32, 164.55, 162.09, 154.80, 137.07, 132.36, 132.28, 131.77, 129.44, 129.36, 127.25, 121.29, 120.02, 116.47, 116.38, 116.25, 115.68, 115.45, 111.62, 58.14, 53.08(2C), 52.79(2C), 52.04, 41.65, 15.62, 12.41. MS (ESI) m/z (%): 519.12 [(M+H)⁺, 100].

(*E*)-*N'*-(4-chlorobenzylidene)-1-ethyl-5-(4-((4-ethylpiperazin-1-yl)methyl)thiazol-2-yl)-1*H*-indole-3-carbohydrazide (**34**). mp 200-202 °C. ¹H NMR (400 MHz, DMSO) δ 11.60 (s, 1H), 8.84 (s, 1H), 8.39 (s, 2H), 7.84 (dd, $J = 8.6, 1.7$ Hz, 1H), 7.76 (d, $J = 8.5$ Hz, 2H), 7.70 (d, $J = 8.7$ Hz, 1H), 7.53 (d, $J = 8.5$ Hz, 2H), 7.41 (s, 1H), 4.35 (q, $J = 6.8$ Hz, 2H), 3.65 (s, 2H), 2.43 (m, 6H), 2.34 (dd, $J = 14.0, 6.9$ Hz, 4H), 1.47 (t, $J = 7.2$ Hz, 3H), 0.99 (t, $J = 7.2$ Hz, 3H). ¹³C NMR (151 MHz, DMSO) δ 168.31, 154.75, 137.16, 134.48, 134.12, 132.54, 130.01, 129.40(2C), 128.91(2C), 127.27, 121.32, 120.01, 119.96, 119.09, 116.44, 111.66, 102.11, 58.10, 52.98(2C), 52.75(2C), 52.03, 41.66, 15.62, 12.34. MS (ESI) m/z (%): 534.74 [(M+H)⁺, 50].

(*E*)-1-ethyl-5-(4-((4-ethylpiperazin-1-yl)methyl)thiazol-2-yl)-*N'*-(1-(4-fluorophenyl)ethylidene)-1*H*-indole-3-carbohydrazide (**35**). mp 214-216 °C. ¹H NMR (400 MHz, DMSO) δ 10.38 (s, 1H), 8.82 (s, 1H), 8.42 (s, 1H), 7.92 – 7.86 (m, 2H), 7.84 (d, $J = 8.5$ Hz, 1H), 7.70 (d, $J = 8.7$ Hz, 1H), 7.43 (s, 1H), 7.28 (t, $J = 8.8$ Hz, 2H), 4.33 (q, $J = 7.3$ Hz, 2H), 3.67 (s, 2H), 2.52 (s, 4H), 2.47 – 2.42 (m, 6H), 2.39 (s, 3H), 1.46 (t, $J = 7.2$ Hz, 3H), 1.01 (t, $J = 6.7$ Hz, 3H). MS (ESI) m/z (%): 533.21 [(M+H)⁺, 100].

(*E*)-*N'*-(4-fluorobenzylidene)-1-methyl-5-(4-(morpholinomethyl)thiazol-2-yl)-1*H*-indole-3-carbohydrazide (**36**). mp 221-223 °C. ¹H NMR (600 MHz, DMSO) δ 11.57 (s, 1H), 8.84 (s, 1H), 8.36 (s, 2H), 7.86 (dd, $J = 8.6, 1.6$ Hz, 1H), 7.80 (dd, $J = 8.2, 5.8$ Hz, 2H), 7.66 (d, $J = 8.6$ Hz, 1H), 7.46 (s, 1H), 7.31 (t, $J = 8.6$ Hz, 2H), 3.94 (s, 4H), 3.66 (s, 3H), 3.61 (m, 6H). MS (ESI) m/z (%): 478.32 [(M+H)⁺, 100].

(*E*)-*N'*-(4-chlorobenzylidene)-1-methyl-5-(4-(morpholinomethyl)thiazol-2-yl)-1*H*-indole-3-carbohydrazide (**37**). mp 241-243 °C. ¹H NMR (400 MHz, DMSO) δ 11.57 (s, 1H), 8.84 (s, 1H), 8.31 (s, 2H), 7.86 (d, $J = 8.5$ Hz, 1H), 7.77 (d, $J = 8.3$ Hz, 2H), 7.65 (d, $J = 8.6$ Hz, 1H), 7.53 (d, $J = 8.3$ Hz, 2H), 7.45 (s, 1H), 3.94 (s, 3H), 3.65 (s, 2H), 3.61 (m, $J = 4.0$ Hz, 4H), 2.50–2.45 (m, 4H). ¹³C NMR (151 MHz, DMSO) δ 168.42, 154.36, 144.07, 142.52, 137.94, 136.62, 134.47, 134.08,

1
2
3
4 131.63, 129.39(2C), 128.96(2C), 128.79, 127.24, 121.34, 119.88, 116.67, 111.66, 66.66(2C), 58.47, 53.65(2C), 33.84. MS
5 (ESI) m/z (%): 494.33 [(M+H)⁺, 75].

6
7 (E)-N'-(benzo[d][1,3]dioxol-5-ylmethylene)-1-methyl-5-(4-(morpholinomethyl)thiazol-2-yl)-1H-indole-3-carbohydrazide
8
9 (38). mp 173-175 °C. ¹H NMR (600 MHz, DMSO) δ 11.47 (s, 1H), 8.82 (s, 1H), 8.28 (m, 2H), 7.85 (dd, *J* = 8.6, 1.6 Hz,
10 1H), 7.65 (d, *J* = 8.6 Hz, 1H), 7.45 (s, 1H), 7.33 (d, *J* = 1.4 Hz, 1H), 7.17 (d, *J* = 7.8 Hz, 1H), 7.00 (d, *J* = 7.9 Hz, 1H), 6.10
11 (s, 2H), 3.93 (s, 3H), 3.65 (s, 2H), 3.62–3.59 (m, 4H), 2.49–2.47 (m, 4H). MS (ESI) m/z (%): 504.02 [(M+H)⁺, 100].

12
13 (E)-N'-(4-fluorobenzylidene)-1-methyl-5-(4-((4-methylpiperazin-1-yl)methyl)thiazol-2-yl)-1H-indole-3-carbohydrazide
14
15 (39). mp 201-203 °C. ¹H NMR (400 MHz, DMSO) δ 11.55 (s, 1H), 8.84 (s, 1H), 8.33 (s, 2H), 7.85 (dd, *J* = 8.6, 1.6 Hz,
16 1H), 7.81 (dd, *J* = 8.5, 5.7 Hz, 2H), 7.65 (d, *J* = 8.6 Hz, 1H), 7.41 (s, 1H), 7.31 (p, *J* = 7.2 Hz, 2H), 3.94 (s, 3H), 3.65 (s,
17 2H), 2.50–2.46 (s, 3H), 2.38 (m, 4H), 2.18 (m, 4H). ¹³C NMR (101 MHz, DMSO) δ 167.80, 163.99, 161.54, 154.22, 137.39,
18
19 131.86, 131.19, 128.93, 128.85, 126.68, 120.75, 119.51, 119.41, 115.90(2C), 115.69, 115.29, 111.06, 57.54, 54.54(2C),
20
21 52.36(2C), 45.52, 33.27. MS (ESI) m/z (%): 490.67 [(M+H)⁺, 43].

22
23 (E)-N'-(1-(4-fluorophenyl)ethylidene)-1-methyl-5-(4-((4-methylpiperazin-1-yl)methyl)thiazol-2-yl)-1H-indole-3-
24
25 carbohydrazide (40). mp 226-228 °C. ¹H NMR (400 MHz, DMSO) δ 10.36 (s, 1H), 8.82 (s, 1H), 8.36 (s, 1H), 7.89 (dd, *J*
26
27 = 8.6, 5.6 Hz, 2H), 7.85 (dd, *J* = 8.6, 1.7 Hz, 1H), 7.65 (d, *J* = 8.6 Hz, 1H), 7.42 (s, 1H), 7.28 (t, *J* = 8.9 Hz, 2H), 3.92 (s,
28
29 3H), 3.82 (s, 2H), 3.65 (s, 3H), 2.39 (m, 4H), 2.38 (s, 3H), 2.19 (m, 4H). ¹³C NMR (101 MHz, DMSO) δ 167.84, 154.15,
30
31 137.28, 134.98, 131.08, 128.37, 128.28, 128.09, 126.62, 120.67, 119.50, 119.38, 118.43, 115.90, 115.29, 115.08, 111.03,
32
33 110.19, 101.31, 57.48, 54.48(2C), 52.24(2C), 45.41, 33.21, 13.92. MS (ESI) m/z (%): 505.30 [(M+H)⁺, 100].

34
35 (E)-N'-(benzo[d][1,3]dioxol-5-ylmethylene)-1-methyl-5-(4-((4-methylpiperazin-1-yl)methyl)thiazol-2-yl)-1H-indole-3-
36
37 carbohydrazide (41). mp 228-230 °C. ¹H NMR (400 MHz, DMSO) δ 11.46 (s, 1H), 8.83 (s, 1H), 8.27 (s, 2H), 7.85 (dd, *J*
38
39 = 8.6, 1.7 Hz, 1H), 7.65 (d, *J* = 8.6 Hz, 1H), 7.41 (s, 1H), 7.34 (s, 1H), 7.17 (d, *J* = 8.1 Hz, 1H), 7.00 (d, *J* = 8.0 Hz, 1H),
40
41 6.10 (s, 2H), 3.93 (s, 3H), 3.64 (s, 2H), 2.50–2.48 (m, 4H), 2.37 (m, 4H), 2.17 (s, 3H). MS (ESI) m/z (%): 517.14 [(M+H)⁺,
42
43 100].

44
45 (E)-1-ethyl-N'-(4-fluorobenzylidene)-5-(4-((4-hydroxypiperidin-1-yl)methyl)thiazol-2-yl)-1H-indole-3-carbohydrazide
46
47 (42). mp 163-165 °C. ¹H NMR (600 MHz, DMSO) δ 11.59 (s, 1H), 8.86 (s, 1H), 8.37 (s, 2H), 7.84 (dd, *J* = 8.6, 1.6 Hz,
48
49 1H), 7.80 (dd, *J* = 8.5, 5.7 Hz, 2H), 7.70 (d, *J* = 8.6 Hz, 1H), 7.41 (s, 1H), 7.32 (t, *J* = 8.7 Hz, 2H), 4.58 (s, 1H), 4.35 (s,
50
51 2H), 3.65 (s, 2H), 3.47 (s, 1H), 2.81 (s, 2H), 2.18 (s, 2H), 1.74 (d, *J* = 9.7 Hz, 2H), 1.47 (t, *J* = 7.2 Hz, 3H), 1.45–1.41 (m,
52
53 2H). ¹³C NMR (151 MHz, DMSO) δ 167.75, 163.61, 161.97, 154.54, 152.44, 136.51, 131.24, 128.87(2C), 128.82(2C),
54
55 126.74, 120.75, 119.52, 115.86(2C), 115.72(2C), 111.04, 66.09, 57.62, 50.81(2C), 41.10, 34.26(2C), 15.05. MS (ESI) m/z
56
57 (%): 506.43 [(M+H)⁺, 100].
58
59
60

1
2
3
4 (*E*)-*N'*-(4-chlorobenzylidene)-1-ethyl-5-(4-((4-hydroxypiperidin-1-yl)methyl)thiazol-2-yl)-1*H*-indole-3-carbohydrazide
5
6 (**43**). mp 143-145 °C. ¹H NMR (600 MHz, DMSO) δ 11.66 (s, 1H), 8.84 (s, 1H), 8.39 (s, 2H), 7.84 (d, *J* = 8.4 Hz, 1H), 7.77
7
8 (d, *J* = 6.9 Hz, 2H), 7.70 (d, *J* = 8.5 Hz, 1H), 7.54 (d, *J* = 6.9 Hz, 2H), 7.42 (s, 1H), 4.58 (s, 1H), 4.35 (s, 2H), 3.67 (s, 2H),
9
10 3.48 (s, 1H), 2.82 (s, 2H), 2.20 (s, 2H), 1.73 (s, 2H), 1.47 (t, *J* = 7.1 Hz, 3H), 1.43 (s, 2H). MS (ESI) *m/z* (%): 522.00
11 [(M+H)⁺, 100].

12
13 (*E*)-1-ethyl-*N'*-(1-(4-fluorophenyl)ethylidene)-5-(4-((4-hydroxypiperidin-1-yl)methyl)thiazol-2-yl)-1*H*-indole-3-
14
15 carbohydrazide (**44**). mp 191-193 °C. ¹H NMR (600 MHz, DMSO) δ 10.40 (s, 1H), 8.83 (s, 1H), 8.43 (s, 1H), 7.90 (dd, *J* =
16
17 7.7, 6.0 Hz, 2H), 7.84 (dd, *J* = 8.6, 1.7 Hz, 1H), 7.70 (d, *J* = 8.6 Hz, 1H), 7.41 (s, 1H), 7.28 (t, *J* = 8.8 Hz, 2H), 4.58 (s,
18
19 1H), 4.33 (q, *J* = 7.2 Hz, 2H), 3.65 (s, 2H), 3.47 (s, 1H), 2.81 (s, 2H), 2.39 (s, 3H), 2.19 (s, 2H), 1.74 (d, *J* = 9.8 Hz, 2H),
20
21 1.46 (t, *J* = 7.2 Hz, 3H), 1.40 (m, 2H). ¹³C NMR (101 MHz, DMSO) δ 168.35, 164.35, 161.90, 154.99, 136.92, 135.56,
22
23 135.53, 128.88, 128.80, 128.25, 127.19, 121.21, 120.04, 116.34, 116.31, 115.84, 115.62, 111.57, 108.74, 66.62, 58.10,
24
25 51.35, 41.60, 34.77, 15.60, 14.32. MS (ESI) *m/z* (%): 520.42 [(M+H)⁺, 100].

26
27 (*E*)-*N'*-(benzo[*d*][1,3]dioxol-5-ylmethylene)-1-ethyl-5-(4-((4-hydroxypiperidin-1-yl)methyl)thiazol-2-yl)-1*H*-indole-3-
28
29 carbohydrazide (**45**). mp 166-168 °C. ¹H NMR (600 MHz, DMSO) δ 11.52 (s, 1H), 8.83 (s, 1H), 8.34 (s, 2H), 7.84 (d, *J* =
30
31 8.5 Hz, 1H), 7.70 (d, *J* = 8.6 Hz, 1H), 7.46 (s, 1H), 7.33 (s, 1H), 7.16 (d, *J* = 7.4 Hz, 1H), 7.01 (d, *J* = 7.9 Hz, 1H), 6.10 (s,
32
33 2H), 4.63 (s, 1H), 4.34 (s, 2H), 3.72 (s, 2H), 3.51 (s, 1H), 3.35 (s, 2H), 2.87 (s, 2H), 2.26 (s, 2H), 1.75 (s, 2H), 1.47 (t, *J* =
34
35 7.2 Hz, 3H). MS (ESI) *m/z* (%): 532.45 [(M+H)⁺, 100].

36
37 (*S,E*)-1-ethyl-*N'*-(4-fluorobenzylidene)-5-(4-((2-(hydroxymethyl)pyrrolidin-1-yl)methyl)thiazol-2-yl)-1*H*-indole-3-
38
39 carbohydrazide (**46**). mp 147-149 °C. ¹H NMR (600 MHz, DMSO) δ 11.56 (s, 1H), 8.83 (s, 1H), 8.36 (s, 2H), 7.84 (dd, *J* =
40
41 8.6, 1.7 Hz, 1H), 7.80 (dd, *J* = 8.6, 5.6 Hz, 2H), 7.70 (d, *J* = 8.7 Hz, 1H), 7.42 (s, 1H), 7.32 (t, *J* = 8.8 Hz, 2H), 4.35 (s,
42
43 2H), 4.13 (d, *J* = 14.2 Hz, 1H), 3.71 (d, *J* = 14.2 Hz, 1H), 3.47 (dd, *J* = 10.6, 4.7 Hz, 1H), 3.32 (dd, *J* = 10.6, 6.4 Hz, 1H),
44
45 3.03 (dt, *J* = 9.2, 4.6 Hz, 1H), 2.71 (s, 1H), 2.40 (dd, *J* = 16.5, 8.2 Hz, 1H), 1.91 (s, 1H), 1.84 (dq, *J* = 12.2, 8.2 Hz, 1H),
46
47 1.69 – 1.62 (m, 2H), 1.58 (dt, *J* = 19.1, 6.5 Hz, 1H), 1.47 (t, *J* = 7.3 Hz, 3H). ¹³C NMR (151 MHz, DMSO) δ 168.20,
48
49 164.14, 162.51, 156.23, 147.63, 144.36, 137.01, 131.77, 129.42, 129.37, 127.30, 121.27, 120.05, 120.01, 116.42, 116.27,
50
51 115.70, 115.51, 111.60, 65.00, 64.55, 54.59, 54.51, 41.64, 28.45, 23.14, 15.61. MS (ESI) *m/z* (%): 506.43 [(M+H)⁺, 100].

52
53 (*S,E*)-1-ethyl-*N'*-(1-(4-fluorophenyl)ethylidene)-5-(4-((2-(hydroxymethyl)pyrrolidin-1-yl)methyl)thiazol-2-yl)-1*H*-
54
55 indole-3-carbohydrazide (**47**). mp 185-187 °C. ¹H NMR (400 MHz, DMSO) δ 10.39 (s, 1H), 8.83 (s, 1H), 8.43 (s, 1H),
56
57 7.93 – 7.87 (m, 2H), 7.84 (d, *J* = 8.7 Hz, 1H), 7.70 (d, *J* = 8.6 Hz, 1H), 7.45 (s, 1H), 7.28 (t, *J* = 8.7 Hz, 2H), 4.39 – 4.28
58
59 (m, 2H), 4.17 (d, *J* = 13.7 Hz, 1H), 3.76 (d, *J* = 12.3 Hz, 1H), 3.49 (d, *J* = 6.0 Hz, 1H), 3.48 (d, *J* = 4.3 Hz, 1H), 3.06 (s,
60
1H), 2.78 (s, 1H), 2.39 (s, 3H), 1.85 (d, *J* = 9.7 Hz, 1H), 1.67 (s, 2H), 1.63 – 1.55 (m, 1H), 1.46 (t, *J* = 7.1 Hz, 3H). ¹³C

1
2
3
4 NMR (101 MHz, DMSO) δ 168.20, 164.18, 161.73, 155.70, 155.53, 136.75, 135.38, 135.36, 128.72, 128.64, 128.03,
5
6 127.01, 121.03, 119.89, 116.00, 115.67, 115.46, 111.41, 108.60, 65.04, 64.07, 54.43, 54.21, 41.43, 28.15, 22.92, 15.45,
7
8 14.28. MS (ESI) m/z (%): 520.42 [(M+H)⁺, 100]. HRMS (ESI) m/z calculated for C₂₈H₃₁FN₅O₂S [M+H]⁺: 520.2104. Found:
9
10 520.2187.

11
12 (*S,E*)-*N'*-(benzo[*d*][1,3]dioxol-5-ylmethylene)-1-ethyl-5-(4-((2-(hydroxymethyl)pyrrolidin-1-yl)methyl)thiazol-2-yl)-1*H*-
13
14 indole-3-carbohydrazide (**48**). mp 128-130 °C. ¹H NMR (400 MHz, DMSO) δ 11.49 (s, 1H), 8.85 (s, 1H), 8.35 (s, 1H), 7.85
15
16 (d, *J* = 8.5 Hz, 1H), 7.69 (d, *J* = 8.6 Hz, 1H), 7.44 (s, 1H), 7.34 (s, 1H), 7.17 (d, *J* = 7.8 Hz, 1H), 7.00 (d, *J* = 7.9 Hz, 1H),
17
18 6.11 (s, 2H), 4.33 (s, 2H), 4.18 (d, *J* = 14.2 Hz, 1H), 3.76 (d, *J* = 14.1 Hz, 1H), 3.50 (dd, *J* = 10.6, 4.5 Hz, 1H), 3.40 – 3.32
19
20 (m, 1H), 3.10 – 3.01 (m, 1H), 2.78 (s, 1H), 2.47 (d, *J* = 8.3 Hz, 1H), 1.92 (s, 1H), 1.85 (dd, *J* = 19.0, 8.2 Hz, 1H), 1.65 (dd,
21
22 *J* = 20.8, 6.7 Hz, 2H), 1.64 – 1.54 (m, 1H), 1.47 (t, *J* = 7.1 Hz, 3H). ¹³C NMR (101 MHz, DMSO) δ 172.48, 168.36, 155.61,
23
24 149.20, 148.47, 137.03, 129.59, 127.20, 123.34, 121.23, 120.38, 120.09, 120.03, 116.10, 111.56, 110.71, 108.93, 107.14,
25
26 105.48, 101.94, 65.21, 64.24, 54.59, 54.38, 41.60, 28.31, 23.09, 15.58. MS (ESI) m/z (%): 532.45 [(M+H)⁺, 100].

27
28 (*E*)-1-ethyl-*N'*-(4-fluorobenzylidene)-5-(4-((2-hydroxyethyl)piperazin-1-yl)methyl)thiazol-2-yl)-1*H*-indole-3-
29
30 carbohydrazide (**49**). mp 133-135 °C. ¹H NMR (400 MHz, DMSO) δ 11.55 (s, 1H), 8.84 (s, 1H), 8.38 (s, 2H), 7.83 (m,
31
32 1H), 7.80 (m, 2H), 7.70 (d, *J* = 8.6 Hz, 1H), 7.41 (s, 1H), 7.31 (s, 2H), 4.36 (m, 2H), 4.34 (m, 2H), 3.65 (m, 2H), 3.49 (t, *J*
33
34 = 6.7 Hz, 2H), 2.50 (m, 4H), 2.42 (m, 4H), 1.47 (t, *J* = 6.9 Hz, 3H). MS (ESI) m/z (%): 535.41 [(M+H)⁺, 100].

35
36 (*E*)-*N'*-(4-chlorobenzylidene)-1-ethyl-5-(4-((2-hydroxyethyl)piperazin-1-yl)methyl)thiazol-2-yl)-1*H*-indole-3-
37
38 carbohydrazide (**50**). mp 157-159 °C. ¹H NMR (400 MHz, DMSO) δ 11.64 (s, 1H), 8.83 (s, 1H), 8.42 (s, 2H), 7.84 (d, *J* =
39
40 8.2 Hz, 1H), 7.76 (d, *J* = 8.3 Hz, 2H), 7.70 (d, *J* = 8.7 Hz, 1H), 7.54 (d, *J* = 8.3 Hz, 2H), 7.41 (s, 1H), 4.36 (s, 2H), 4.34 (m,
41
42 2H), 3.64 (s, 2H), 3.48 (s, 2H), 2.45 (m, 4H), 2.38 (t, *J* = 6.2 Hz, 4H), 1.47 (t, *J* = 7.1 Hz, 3H). MS (ESI) m/z (%): 551.42
43
44 [(M+H)⁺, 100].

45
46 (*E*)-1-ethyl-*N'*-(1-(4-fluorophenyl)ethylidene)-5-(4-((2-hydroxyethyl)piperazin-1-yl)methyl)thiazol-2-yl)-1*H*-indole-3-
47
48 carbohydrazide (**51**). mp 131-133 °C. ¹H NMR (600 MHz, DMSO) δ 10.39 (s, 1H), 8.82 (s, 1H), 8.43 (s, 1H), 7.89 (dd, *J* =
49
50 8.1, 5.8 Hz, 2H), 7.83 (dd, *J* = 8.6, 1.7 Hz, 1H), 7.70 (d, *J* = 8.6 Hz, 1H), 7.42 (s, 1H), 7.30–7.27 (m, 2H), 4.44 (s, 1H),
51
52 4.33 (q, *J* = 7.2 Hz, 2H), 3.66 (s, 2H), 3.50 (s, 2H), 3.33 (s, 2H), 2.52 (m, 4H), 2.48–2.42 (m, 4H), 2.39 (s, 3H), 1.46 (t, *J*
53
54 = 7.2 Hz, 3H). MS (ESI) m/z (%): 549.46 [(M+H)⁺, 100].

55
56 (*E*)-*N'*-(benzo[*d*][1,3]dioxol-5-ylmethylene)-1-ethyl-5-(4-((2-hydroxyethyl)piperazin-1-yl)methyl)thiazol-2-yl)-1*H*-
57
58 indole-3-carbohydrazide (**52**). mp 157-159 °C. ¹H NMR (600 MHz, DMSO) δ 11.47 (s, 1H), 8.82 (s, 1H), 8.31 (s, 2H),
59
60 7.83 (dd, *J* = 8.6, 1.7 Hz, 1H), 7.70 (d, *J* = 8.7 Hz, 1H), 7.42 (s, 1H), 7.32 (s, 1H), 7.16 (d, *J* = 7.7 Hz, 1H), 7.01 (d, *J* = 8.0
Hz, 1H), 6.10 (s, 2H), 4.45 (s, 1H), 4.34 (s, 2H), 3.66 (s, 2H), 3.50 (s, 2H), 3.34 (s, 2H), 2.52 (m, 4H), 2.49–2.37 (m, 4H),

1
2
3
4 1.47 (t, $J = 7.2$ Hz, 3H). MS (ESI) m/z (%): 561.44 [(M+H)⁺, 100].

5 6 4.1.11 General procedure for preparation of intermediates **18i-2~18l-2**

7
8 The indole-3-carboxylic acid intermediates with a -OH containing amines (**18i~18l**, 3 mmol) were introduced to a
9 mixture of TEA (7.5 mmol) and DMAP (0.3 mmol) in 20 mL DCM and stirred for 10 min. Subsequently, acetic anhydride
10 (4.5 mmol) was added slowly and the system was kept at ambient temperature for 1.5 h. Water (20 mL) was added to the
11 mixture and the organic phase was separated, concentrated to give yellow products **18i-2~18l-2** in high yields (81%~93%).

12 13 14 4.1.12 General procedure for preparation of target compounds **53-69**

15
16 The carboxylic acid intermediates **18i-2~18l-2** (2 mmol) were added to a mixture of TEA (4 mmol) and DPPA (2.4
17 mmol) in toluene. The mixtures were refluxed for 30 min before the addition of corresponding benzyl alcohols. After
18 the reaction finished as indicated by TLC results, the toluene was removed in vacuum followed by extraction with
19 DCM from water. The crude ester intermediates (1 mmol) were dissolved in dioxane (3 mL) followed by the addition of
20 2 M aqueous NaOH (10 mL). The mixture was kept at 50 °C for 2 h after which the solvent was removed in reduced
21 pressure. More water (30 mL) was added and the acquired mixture was extracted with DCM (20 × 2) to give the crude
22 materials. Finally, the raw materials were purified by column chromatography/*p*-TLC (DCM: MeOH= 35~12:1) to give
23 final products **53~69** in high yields (85%~93%).

24
25 3,5-dichlorobenzyl (1-ethyl-5-(4-((4-hydroxypiperidin-1-yl)methyl)thiazol-2-yl)-1*H*-indol-3-yl)carbamate (**53**). mp 67-69
26 °C. ¹H NMR (600 MHz, DMSO) δ 9.96 (s, 1H), 8.47 (s, 1H), 7.73 (dd, $J = 8.6, 1.6$ Hz, 1H), 7.60 (s, 2H), 7.54 (s, 2H), 7.52
27 (d, $J = 8.7$ Hz, 1H), 7.35 (dd, $J = 3.3, 2.5$ Hz, 1H), 5.20 (s, 2H), 4.56 (s, 1H), 4.20 (q, $J = 7.2$ Hz, 2H), 3.60 (s, 2H), 3.46
28 (s, 1H), 2.79 (s, 2H), 2.15 (s, 2H), 1.73 (d, $J = 9.9$ Hz, 2H), 1.42 (dd, $J = 13.1, 5.9$ Hz, 2H), 1.34 (t, $J = 7.2$ Hz, 3H). ¹³C
29 NMR (101 MHz, DMSO) δ 168.75, 154.84, 153.97, 141.81, 134.57, 134.47, 127.87, 126.71(2C), 125.32, 124.63, 121.37,
30 120.51, 118.61, 117.45, 115.86, 115.74, 110.59, 66.74, 64.69, 58.27, 51.43(2C), 40.87, 34.85(2C), 15.87. MS (ESI) m/z
31 (%): 559.07 [(M+H)⁺, 98].

32
33 (*R*)-1-(*p*-tolyl)ethyl (1-ethyl-5-(4-((4-hydroxypiperidin-1-yl)methyl)thiazol-2-yl)-1*H*-indol-3-yl)carbamate (**54**). mp 170-
34 172 °C. ¹H NMR (400 MHz, DMSO) δ 9.83 (s, 1H), 8.49 (s, 1H), 7.72 (dd, $J = 8.7, 1.5$ Hz, 1H), 7.55 (s, 1H), 7.49 (d, $J =$
35 8.7 Hz, 1H), 7.34 (t, $J = 3.6$ Hz, 3H), 7.19 (d, $J = 7.6$ Hz, 2H), 5.79 (q, $J = 6.5$ Hz, 1H), 4.56 (d, $J = 4.0$ Hz, 1H), 4.17 (q,
36 $J = 7.1$ Hz, 2H), 3.60 (s, 2H), 3.46 (dd, $J = 8.3, 4.2$ Hz, 1H), 2.85 – 2.73 (m, 2H), 2.29 (s, 3H), 2.15 (t, $J = 9.9$ Hz, 2H),
37 1.73 (d, $J = 9.7$ Hz, 2H), 1.55 (d, $J = 6.5$ Hz, 3H), 1.42 (td, $J = 12.8, 3.5$ Hz, 2H), 1.31 (t, $J = 7.0$ Hz, 3H). ¹³C NMR (101
38 MHz, DMSO) δ 168.81, 154.91, 153.83, 139.96, 137.21, 134.42, 129.37(2C), 126.24(2C), 124.54, 121.30, 120.39, 118.27,
39 117.66, 116.18, 115.62, 110.46, 72.28, 66.75, 58.30, 51.44(2C), 40.81, 34.89(2C), 22.90, 21.16, 15.83. MS (ESI) m/z (%):
40 519.44 [(M+H)⁺, 100].

1
2
3
4 Benzyl (1-ethyl-5-(4-((4-hydroxypiperidin-1-yl)methyl)thiazol-2-yl)-1*H*-indol-3-yl)carbamate (**55**). mp 75-77 °C. ¹H
5 NMR (400 MHz, DMSO) δ 9.87 (s, 1H), 8.47 (s, 1H), 7.73 (dd, *J* = 8.7, 1.5 Hz, 1H), 7.60 (s, 1H), 7.50 (d, *J* = 8.7 Hz, 1H),
6 7.47 (d, *J* = 7.1 Hz, 2H), 7.41 (t, *J* = 7.3 Hz, 2H), 7.36 (d, *J* = 7.0 Hz, 1H), 7.33 (s, 1H), 5.19 (s, 2H), 4.55 (d, *J* = 4.0 Hz,
7 1H), 4.19 (q, *J* = 7.1 Hz, 2H), 3.60 (s, 2H), 3.49–3.42 (m, 1H), 2.81–2.74 (m, 2H), 2.14 (t, *J* = 10.0 Hz, 2H), 1.72 (d, *J* =
8 9.9 Hz, 2H), 1.41 (td, *J* = 12.8, 3.5 Hz, 2H), 1.34 (t, *J* = 7.2 Hz, 3H). ¹³C NMR (151 MHz, DMSO) δ 168.73, 154.86,
9 154.29, 137.36, 134.40, 128.85(2C), 128.42(2C), 128.38, 124.53, 121.34, 120.38, 118.41, 117.54, 116.04, 115.61, 110.47,
10 66.21, 58.25, 51.39(2C), 40.80, 40.49, 34.83(2C), 15.82. MS (ESI) *m/z* (%): 490.77 [(*M*+*H*)⁺, 40].

11
12
13
14
15
16
17 (*R*)-1-(2-chlorophenyl)ethyl (1-ethyl-5-(4-((4-hydroxypiperidin-1-yl)methyl)thiazol-2-yl)-1*H*-indol-3-yl)carbamate (**56**).
18 mp 103-105 °C. ¹H NMR (400 MHz, DMSO) δ 9.98 (s, 1H), 8.50 (s, 1H), 7.73 (d, *J* = 8.6 Hz, 1H), 7.62 (d, *J* = 7.4 Hz,
19 1H), 7.56 (s, 1H), 7.51–7.46 (m, 2H), 7.43 (t, *J* = 7.5 Hz, 1H), 7.34 (d, *J* = 8.7 Hz, 2H), 6.09 (q, *J* = 6.5 Hz, 1H), 4.57 (d,
20 *J* = 2.8 Hz, 1H), 4.16 (dd, *J* = 14.0, 6.9 Hz, 2H), 3.62 (s, 2H), 3.48 (s, 1H), 2.81 (d, *J* = 10.3 Hz, 2H), 2.17 (s, 2H), 1.74 (d,
21 *J* = 9.8 Hz, 2H), 1.56 (d, *J* = 6.4 Hz, 3H), 1.43 (m, 2H), 1.31 (t, *J* = 7.1 Hz, 3H). ¹³C NMR (101 MHz, DMSO) δ 168.81,
22 154.85, 153.44, 140.64, 134.42, 131.30, 129.87, 129.67, 128.20, 126.92, 124.57, 121.27, 120.45, 118.40, 117.56, 115.97,
23 115.71, 110.51, 69.29, 66.72, 58.24, 51.42(2C), 40.82, 34.83(2C), 21.55, 15.82. MS (ESI) *m/z* (%): 539.22 [(*M*+*H*)⁺, 100].

24
25
26
27
28
29
30
31 2,3-dichlorobenzyl (1-ethyl-5-(4-((4-hydroxypiperidin-1-yl)methyl)thiazol-2-yl)-1*H*-indol-3-yl)carbamate (**57**). mp 76-78
32 °C. ¹H NMR (400 MHz, DMSO) δ 9.99 (s, 1H), 8.47 (s, 1H), 7.73 (d, *J* = 8.7 Hz, 1H), 7.67 (d, *J* = 7.9 Hz, 1H), 7.60 (s,
33 2H), 7.51 (d, *J* = 8.7 Hz, 1H), 7.46 (t, *J* = 7.7 Hz, 1H), 7.35 (s, 1H), 5.31 (s, 2H), 4.56 (s, 1H), 4.20 (dd, *J* = 13.9, 6.8 Hz,
34 2H), 3.62 (s, 2H), 3.47 (s, 1H), 2.79 (s, 2H), 2.17 (s, 2H), 1.73 (d, *J* = 10.0 Hz, 2H), 1.50 – 1.37 (m, 2H), 1.34 (t, *J* = 7.1
35 Hz, 3H). ¹³C NMR (101 MHz, DMSO) δ 168.66, 154.64, 153.80, 137.41, 134.36, 132.28, 130.72, 130.49, 128.72(2C),
36 128.69, 124.49, 121.26, 120.36, 118.48, 117.41, 115.75, 110.36, 66.56, 63.87, 58.06, 51.26(2C), 40.73, 34.64(2C), 15.73.
37 MS (ESI) *m/z* (%): 559.07 [(*M*+*H*)⁺, 98].

38
39
40
41
42
43
44 Benzo[*d*][1,3]dioxol-5-ylmethyl (1-ethyl-5-(4-((4-hydroxypiperidin-1-yl)methyl)thiazol-2-yl)-1*H*-indol-3-yl)carbamate
45 (**58**). mp 64-66 °C. ¹H NMR (400 MHz, DMSO) δ 9.82 (s, 1H), 8.46 (s, 1H), 7.73 (d, *J* = 8.5 Hz, 1H), 7.59 (s, 1H), 7.50
46 (d, *J* = 8.6 Hz, 1H), 7.35 (s, 1H), 7.04 (s, 1H), 6.94 (s, 2H), 6.03 (s, 2H), 5.08 (s, 2H), 4.57 (s, 1H), 4.26 – 4.10 (m, 2H),
47 3.63 (s, 2H), 3.47 (s, 1H), 2.80 (s, 2H), 2.18 (s, 2H), 1.73 (d, *J* = 10.0 Hz, 2H), 1.43 (d, *J* = 9.2 Hz, 2H), 1.34 (t, *J* = 7.0
48 Hz, 3H). ¹³C NMR (101 MHz, DMSO) δ 168.88, 154.64, 154.38, 147.81, 147.54, 134.49, 131.08, 124.58, 122.57, 121.43,
49 120.44, 118.48, 117.65, 116.13, 115.88, 110.55, 109.35, 108.66, 101.54, 66.28, 58.18, 51.39(2C), 40.88, 34.76(2C), 27.33,
50 15.90. MS (ESI) *m/z* (%): 535.25 [(*M*+*H*)⁺, 100].

51
52
53
54
55
56
57
58 3,4-difluorobenzyl (1-ethyl-5-(4-((4-hydroxypiperidin-1-yl)methyl)thiazol-2-yl)-1*H*-indol-3-yl)carbamate (**59**). mp 68-70
59 °C. ¹H NMR (400 MHz, DMSO) δ 9.91 (s, 1H), 8.46 (s, 1H), 7.73 (d, *J* = 8.5 Hz, 1H), 7.60 (s, 1H), 7.51 (dd, *J* = 19.8, 10.9
60

1
2
3
4 Hz, 3H), 7.35 (s, 2H), 5.17 (s, 2H), 4.56 (s, 1H), 4.20 (d, $J = 6.8$ Hz, 2H), 3.61 (s, 2H), 3.47 (s, 1H), 2.79 (m, 2H), 2.16 (m,
5
6 2H), 1.72 (m, 2H), 1.42 (d, $J = 9.4$ Hz, 2H), 1.34 (t, $J = 6.9$ Hz, 3H). ^{13}C NMR (101 MHz,) δ 170.44, 158.66, 143.40,
7
8 142.79, 135.43, 135.41, 134.82, 132.23, 131.48, 129.96, 129.57, 129.43, 129.17, 129.10, 129.03, 127.83, 127.68, 123.48,
9
10 61.36, 60.02, 54.54, 49.03(2C), 40.51, 35.63(2C), 15.34. MS (ESI) m/z (%): 526.74 [(M+H)⁺, 65]. HRMS (ESI) m/z
11
12 calculated for $\text{C}_{27}\text{H}_{29}\text{F}_2\text{N}_4\text{O}_3\text{S}$ [M+H]⁺: 527.1884. Found: 527.1923.

13
14 Benzyl (*S*)-(1-ethyl-5-(4-((2-(hydroxymethyl)pyrrolidin-1-yl)methyl)thiazol-2-yl)-1*H*-indol-3-yl)carbamate (**60**). mp 113-
15
16 115 °C. ^1H NMR (400 MHz, DMSO) δ 9.87 (s, 1H), 8.45 (s, 1H), 7.73 (d, $J = 7.7$ Hz, 1H), 7.60 (s, 1H), 7.51 (d, $J = 8.7$
17
18 Hz, 1H), 7.47 (d, $J = 6.9$ Hz, 2H), 7.44 – 7.39 (m, 2H), 7.34 (dd, $J = 15.1, 6.2$ Hz, 2H), 5.19 (s, 2H), 4.45 (s, 1H), 4.19 (dd,
19
20 $J = 14.0, 6.9$ Hz, 2H), 4.10 (d, $J = 14.2$ Hz, 1H), 3.68 (d, $J = 14.2$ Hz, 1H), 3.46 (dd, $J = 10.3, 4.2$ Hz, 1H), 3.30 (d, $J =$
21
22 10.5 Hz, 1H), 3.05–2.98 (m, 1H), 2.69 (m, 1H), 2.44–2.33 (m, 1H), 1.82 (dd, $J = 19.2, 8.3$ Hz, 1H), 1.70–1.60 (m, 2H),
23
24 1.57 (dd, $J = 12.0, 6.0$ Hz, 1H), 1.34 (t, $J = 7.1$ Hz, 3H). ^{13}C NMR (101 MHz, DMSO) δ 168.78, 155.99, 154.40, 137.46,
25
26 134.51, 128.96(2C), 128.54, 128.49, 126.93, 124.67, 121.45, 120.46, 118.55, 117.67, 116.12, 115.21, 110.58, 66.33, 65.05,
27
28 64.62, 54.68, 54.62, 40.90, 28.52, 23.19, 15.92. MS (ESI) m/z (%): 490.77 [(M+H)⁺, 40].

29
30 (*R*)-1-(*p*-tolyl)ethyl (1-ethyl-5-(4-(((*S*)-2-(hydroxymethyl)pyrrolidin-1-yl)methyl)thiazol-2-yl)-1*H*-indol-3-yl)carbamate
31
32 (**61**). mp 63–65 °C. ^1H NMR (400 MHz, DMSO) δ 9.82 (s, 1H), 8.47 (s, 1H), 7.76 – 7.71 (m, 1H), 7.55 (s, 1H), 7.49 (d, $J =$
33
34 8.7 Hz, 1H), 7.38 (d, $J = 11.2$ Hz, 1H), 7.34 (d, $J = 7.8$ Hz, 2H), 7.20 (dd, $J = 7.6, 3.9$ Hz, 2H), 5.82–5.76 (m, 1H), 4.48 (s,
35
36 1H), 4.17 (dd, $J = 15.3, 8.2$ Hz, 2H), 3.70 (d, $J = 14.1$ Hz, 1H), 3.47 (dd, $J = 10.6, 4.7$ Hz, 1H), 3.32 (dd, $J = 10.5, 6.3$ Hz,
37
38 1H), 3.03 (dd, $J = 8.4, 4.4$ Hz, 1H), 2.73 (s, 1H), 2.42 (d, $J = 7.7$ Hz, 1H), 2.30 (s, 4H), 1.83 (dt, $J = 11.8, 8.3$ Hz, 1H), 1.66
39
40 (dd, $J = 14.3, 7.1$ Hz, 2H), 1.61 (d, $J = 6.5$ Hz, 1H), 1.55 (d, $J = 6.5$ Hz, 3H), 1.32 (t, $J = 7.1$ Hz, 3H). ^{13}C NMR (101 MHz,
41
42 DMSO) δ 168.71, 153.74, 139.85, 137.12, 136.66, 134.32, 129.28(2C), 126.15(2C), 124.45, 121.20, 120.26, 118.22, 117.60,
43
44 116.00, 115.19, 110.37, 72.20, 64.98, 64.36, 54.52, 54.41, 40.72, 28.32, 23.03, 22.78, 21.07, 15.74. MS (ESI) m/z (%):
45
46 519.32 [(M+H)⁺, 100].

47
48 (*R*)-1-(2-chlorophenyl)ethyl (1-ethyl-5-(4-(((*S*)-2-(hydroxymethyl)pyrrolidin-1-yl)methyl)thiazol-2-yl)-1*H*-indol-3-
49
50 yl)carbamate (**62**). mp 63–65 °C. ^1H NMR (400 MHz, DMSO) δ 9.97 (s, 1H), 8.48 (s, 1H), 7.74 (d, $J = 8.6$ Hz, 1H), 7.62
51
52 (d, $J = 7.3$ Hz, 1H), 7.56 (s, 1H), 7.52–7.46 (m, 2H), 7.43 (t, $J = 7.3$ Hz, 1H), 7.36 (d, $J = 7.7$ Hz, 2H), 6.09 (q, $J = 6.4$ Hz,
53
54 1H), 4.47 (s, 1H), 4.23–4.14 (m, 2H), 4.10 (s, 1H), 3.70 (d, $J = 14.1$ Hz, 1H), 3.47 (dd, $J = 10.4, 4.4$ Hz, 1H), 3.32 (d, $J =$
55
56 10.3 Hz, 1H), 3.03 (d, $J = 4.0$ Hz, 1H), 2.72 (s, 1H), 2.42 (d, $J = 7.6$ Hz, 1H), 1.84 (dd, $J = 19.0, 8.2$ Hz, 1H), 1.64 (td, $J =$
57
58 10.2, 6.3 Hz, 2H), 1.61 (d, $J = 6.5$ Hz, 1H), 1.56 (d, $J = 6.4$ Hz, 3H), 1.31 (t, $J = 7.0$ Hz, 3H). ^{13}C NMR (101 MHz, DMSO)
59
60 δ 168.29, 155.28, 152.93, 140.11, 133.90, 130.79, 129.35, 129.15, 127.68, 126.41, 124.09, 120.76, 119.90, 117.92, 117.06,
115.43, 114.74, 109.99, 68.78, 64.54, 63.98, 54.11, 54.02, 40.30, 27.91, 22.61, 21.02, 15.30. MS (ESI) m/z (%): 539.22

1
2
3
4 [(M+H)⁺, 100].

5 2,3-dichlorobenzyl (S)-(1-ethyl-5-(4-((2-(hydroxymethyl)pyrrolidin-1-yl)methyl)thiazol-2-yl)-1*H*-indol-3-yl)carbamate
6
7 (**63**). mp 136-138 °C. ¹H NMR (400 MHz, DMSO) δ 9.98 (s, 1H), 8.46 (s, 1H), 7.75 (d, *J* = 8.3 Hz, 1H), 7.67 (d, *J* = 7.5
8 Hz, 1H), 7.60 (s, 2H), 7.52 (d, *J* = 8.6 Hz, 1H), 7.46 (t, *J* = 7.7 Hz, 1H), 7.40 (s, 1H), 5.31 (s, 2H), 4.20 (d, *J* = 7.0 Hz, 2H),
9 4.15 (d, *J* = 15.4 Hz, 1H), 3.74 (d, *J* = 13.8 Hz, 1H), 3.49 (d, *J* = 4.8 Hz, 1H), 3.47 (d, *J* = 4.5 Hz, 1H), 3.08 (s, 1H), 3.06
10 (s, 1H), 2.79 (s, 1H), 2.49 – 2.44 (m, 1H), 1.94 – 1.79 (m, 1H), 1.67 (m, 2H), 1.59 (dd, *J* = 11.8, 6.1 Hz, 1H), 1.34 (t, *J* =
11 7.1 Hz, 3H). ¹³C NMR (101 MHz, DMSO) δ 168.84, 153.94, 137.52, 134.50, 132.42, 130.87, 130.63, 128.86(2C), 124.61,
12 121.40, 120.46, 119.10, 118.66, 117.60, 115.86, 115.73, 110.58, 65.26, 64.18, 64.01, 54.61, 54.37, 40.87, 28.29, 23.07,
13 15.86. MS (ESI) *m/z* (%): 558.62 [(M+H)⁺,50].

14
15 Benzo[*d*][1,3]dioxol-5-ylmethyl (S)-(1-ethyl-5-(4-((2-(hydroxymethyl)pyrrolidin-1-yl)methyl)thiazol-2-yl)-1*H*-indol-3-
16 yl)carbamate (**64**). mp 129-131 °C. ¹H NMR (400 MHz, DMSO) δ 9.81 (s, 1H), 8.44 (s, 1H), 7.74 (d, *J* = 8.5 Hz, 1H), 7.59
17 (s, 1H), 7.51 (d, *J* = 8.7 Hz, 1H), 7.39 (s, 1H), 7.03 (s, 1H), 6.95 (d, *J* = 3.5 Hz, 2H), 6.03 (s, 2H), 5.08 (s, 2H), 4.57–4.47
18 (m, 1H), 4.23–4.18 (m, 2H), 4.15 (d, *J* = 16.0 Hz, 1H), 3.76 (s, 1H), 3.48 (m, 2H)3.07 (d, *J* = 6.1 Hz, 1H), 2.78 (s, 1H),
19 1.85 (dd, *J* = 19.1, 8.2 Hz, 1H), 1.67 (d, *J* = 6.8 Hz, 2H), 1.58 (dd, *J* = 11.8, 6.1 Hz, 2H), 1.34 (t, *J* = 7.1 Hz, 3H). ¹³C NMR
20 (101 MHz, DMSO) δ 168.96, 154.40, 147.84, 147.57, 134.54, 131.10, 130.11, 124.59, 122.62, 121.45, 120.44, 118.55,
21 117.73, 116.13, 110.60, 109.40, 108.69, 101.57, 66.32, 65.35, 64.23, 54.67, 54.41, 40.91, 29.54, 28.33, 23.13, 15.93. MS
22 (ESI) *m/z* (%): 534.68 [(M+H)⁺,70].

23
24 3,4-difluorobenzyl (S)-(1-ethyl-5-(4-((2-(hydroxymethyl)pyrrolidin-1-yl)methyl)thiazol-2-yl)-1*H*-indol-3-yl)carbamate
25
26 (**65**). mp 146-148 °C. ¹H NMR (400 MHz, DMSO) δ 9.97 (s, 1H), 8.53 (s, 1H), 7.85 (s, 1H), 7.80 (dd, *J* = 8.7, 1.3 Hz, 1H),
27 7.62 (s, 1H), 7.58–7.50 (m, 2H), 7.50–7.43 (m, 1H), 6.99 (d, *J* = 7.1 Hz, 1H), 5.67 (s, 1H), 5.18 (s, 2H), 4.87 (s, 1H), 4.65
28 (d, *J* = 12.4 Hz, 1H), 4.49–4.40 (m, 1H), 4.21 (q, *J* = 7.1 Hz, 2H), 3.72 (s, 3H), 3.34 (s, 1H), 2.12–1.99 (m, 1H), 1.95–1.79
29 (m, 2H), 1.74 (d, *J* = 7.2 Hz, 1H), 1.34 (t, *J* = 7.2 Hz, 3H). ¹³C NMR (151 MHz, DMSO) δ 170.35, 154.11, 153.96, 135.18,
30 134.67, 125.43, 124.09, 123.94, 122.65, 121.37, 118.67, 118.17, 118.08, 117.97, 117.64, 117.53, 116.09, 110.67, 68.27,
31 65.04, 60.14, 54.33, 52.51, 40.90, 26.53, 22.43, 15.87. MS (ESI) *m/z* (%): 526.74 [(M+H)⁺,70].

32
33 3,5-dichlorobenzyl (1-ethyl-5-(4-((2-(2-hydroxyethyl)piperazin-1-yl)methyl)thiazol-2-yl)-1*H*-indol-3-yl)carbamate (**66**).
34
35 mp 80-82 °C. ¹H NMR (400 MHz, DMSO) δ 9.96 (s, 1H), 8.47 (s, 1H), 7.73 (d, *J* = 8.7 Hz, 1H), 7.60 (s, 2H), 7.54 (s, 2H),
36 7.52 (d, *J* = 9.0 Hz, 1H), 7.36 (s, 1H), 5.20 (s, 2H), 4.44 (s, 1H), 4.20 (q, *J* = 6.9 Hz, 2H), 3.62 (s, 2H), 3.49 (t, *J* = 6.1 Hz,
37 2H), 3.42 (s, 2H), 2.49–2.45 (m, 4H), 2.42 (t, *J* = 6.1 Hz, 4H), 1.34 (t, *J* = 7.1 Hz, 3H). ¹³C NMR (101 MHz, DMSO) δ
38 168.87, 154.47, 154.03, 141.87, 134.63, 134.54, 127.94(2C), 126.77(2C), 124.66, 121.44, 120.57, 118.68, 117.52, 116.00,
39 115.92, 110.66, 64.75, 60.66, 58.83, 58.22, 53.62(2C), 53.00(2C), 40.93, 15.94. MS (ESI) *m/z* (%): 588.13 [(M+H)⁺, 100].
40
41
42
43
44
45
46
47
48
49
50
51
52
53
54
55
56
57
58
59
60

2,3-dichlorobenzyl (1-ethyl-5-(4-((4-(2-hydroxyethyl)piperazin-1-yl)methyl)thiazol-2-yl)-1*H*-indol-3-yl)carbamate (**67**). mp 82-84 °C. ¹H NMR (400 MHz, DMSO) δ 10.00 (s, 1H), 8.48 (s, 1H), 7.73 (d, *J* = 8.7 Hz, 1H), 7.67 (d, *J* = 7.3 Hz, 1H), 7.60 (s, 2H), 7.52 (d, *J* = 8.6 Hz, 1H), 7.48–7.43 (m, 1H), 7.35 (s, 1H), 5.31 (s, 2H), 4.42 (s, 1H), 4.20 (d, *J* = 6.9 Hz, 2H), 3.62 (s, 2H), 3.49 (s, 2H), 2.48–2.45 (m, 6H), 2.40 (m, 4H), 1.34 (t, *J* = 7.0 Hz, 3H). ¹³C NMR (101 MHz, DMSO) δ 168.81, 154.43, 153.92, 137.53, 134.47, 132.41, 130.85, 130.63, 130.05, 128.86(2C), 124.60, 121.36, 120.49, 118.59, 117.53, 115.91, 110.58, 64.00, 60.65, 58.82, 58.17, 53.59(2C), 52.99(2C), 40.86, 15.87. MS (ESI) *m/z* (%): 588.13 [(*M*+*H*)⁺, 100].

3,5-dichlorobenzyl (5-(4-((bis(2-hydroxyethyl)amino)methyl)thiazol-2-yl)-1-ethyl-1*H*-indol-3-yl)carbamate (**68**). mp 102-104 °C. ¹H NMR (400 MHz, DMSO) δ 7.73 (t, *J* = 12.3 Hz, 1H), 7.60 (s, 1H), 7.53 (d, *J* = 8.7 Hz, 1H), 7.45 (d, *J* = 1.9 Hz, 1H), 7.42 (s, 2H), 7.35 (s, 1H), 7.16 (s, 1H), 6.97 (s, 1H), 4.89 (s, 2H), 4.85 (s, 2H), 4.51 (d, *J* = 5.6 Hz, 2H), 4.25–4.13 (m, 2H), 3.89 (s, 2H), 3.53 (s, 2H), 3.51 (s, 2H), 2.70 (s, 2H), 1.34 (t, *J* = 5.7 Hz, 3H). MS (ESI) *m/z* (%): 563.03 [(*M*+*H*)⁺, 65].

Benzo[*d*][1,3]dioxol-5-ylmethyl (5-(4-((bis(2-hydroxyethyl)amino)methyl)thiazol-2-yl)-1-ethyl-1*H*-indol-3-yl)carbamate (**69**). mp 93-95 °C. ¹H NMR (400 MHz, DMSO) δ 9.81 (s, 1H), 8.44 (d, *J* = 10.1 Hz, 1H), 7.74 (d, *J* = 8.7 Hz, 1H), 7.60 (d, *J* = 8.6 Hz, 1H), 7.51 (d, *J* = 8.8 Hz, 1H), 7.43 (s, 1H), 7.03 (s, 1H), 6.94 (m, 2H), 6.03 (s, 2H), 5.08 (s, 2H), 4.45 (s, 2H), 4.19 (d, *J* = 7.1 Hz, 2H), 3.88 (s, 2H), 3.55 (d, *J* = 5.8 Hz, 2H), 3.54–3.50 (m, 4H), 2.69 (t, *J* = 6.0 Hz, 2H), 1.34 (t, *J* = 7.2 Hz, 3H). MS (ESI) *m/z* (%): 539.09 [(*M*+*H*)⁺, 50].

4.2 Biological evaluation section

4.2.1 *In vitro* enzymatic activity of target compounds

Starting from 10 μM highest concentration, 10 μL of a diluted series of compounds, 1/10 dilution, were added to the wells. Human ATX protein (Echelon Biosciences, Inc. Salt Lake City, UT) was used at a final concentration of 0.4/0.64 μg/mL. The enzyme was diluted in 50 mM Tris-HCl at pH 8.0, 5 mM KCl, 250 mM NaCl, 1 mM CaCl₂, 1 mM MgCl₂, and 0.1% fatty acid free BSA to a total volume of 20 μL. The enzyme complex was added to compounds followed by incubating for 45 min at room temperature with shaking. The reaction was started from the addition of 20 μL of 1 μM FS-3 (Echelon Biosciences, Inc. Salt Lake City, UT) diluted in the buffer mentioned above. The rate of increase in fluorescence was measured at 37 °C every minute for 30 min using a Multi-Mode Microplate Reader (Thermo Varioskan Flash, excitation 485 nm, emission 528 nm). Data was analyzed using Statistical Product and Service Solutions (SPSS).

4.2.2 *Mouse Model of Pulmonary Fibrosis and Inhibitor Administration Protocol*

All animal studies complied with the ARRIVE guidelines, and all experiments on animals were performed according to the guidelines of the Animal Experimental Ethics Committee of Shenyang Pharmaceutical University. C57BL/6J male mice, 8~9 weeks old, average weight 23.8 g, were administered at day +1 with 3.5 mg/kg of bleomycin sulfate diluted in

1
2
3
4 50 μ L saline 0.9% orotracheally or equal volume of saline 0.9 % (control group, n =5). Animals were blindly randomized
5
6 to receive inhibitors (20 or 60 mg/kg, n =5) or vehicle (1 \times PBS with 5% Tween 80, n =5), once daily for 31 days (from day
7
8 -3 to 28) by tracheal administration. At day +28, all mice were undergoing euthanasia and the lung tissues were collected
9
10 for further analysis.

11 4.2.3 Lung Histopathology analysis

12
13 Lung tissues embedded in paraformaldehyde (4 μ m slices) were stained with haematoxylin/eosin (H&E) or Masson's
14
15 trichrome. Histopathologic analysis of fibrosis was performed in a blinded fashion using the modified Ashcroft score.
16
17 Imaging was performed using a Nikon Eclipse E800 microscope (Nikon Corp., Shinagawa-ku, Japan) attached to a Q
18
19 Imaging EXI Aqua digital camera, using the Q-Capture Pro 7 software.

21 4.2.4 *In vivo* enzymatic activity of **59** and **66**

22
23 *In vivo* ATX lysoPLD activity was measured by the fluorescence excitation through the cleavage of the phospholipid
24
25 bond in the artificial substrate FS-3. Briefly, 10 μ L of the lung homogenate was used as the test sample. A control sample
26
27 was prepared to account for base line absorbance, using 10 μ L lung homogenate in the control group mice and lysoPLD
28
29 buffer alone. The reaction was started from the addition of 20 μ L of 1 μ M FS-3 (Echelon Biosciences, Inc. Salt Lake City,
30
31 UT). The absorbance (OD value) was read with a Multi-Mode Microplate Reader (Thermo Varioskan Flash, excitation 485
32
33 nm, emission 528 nm). The relative absorbance values were directly utilized for an intuitive analysis of the *in vivo* ATX
34
35 inhibitory effects of compounds **59**, **66** and GLPG-1690.

37 4.3 Molecular modeling study

38
39 The molecular docking was performed with Schrodinger 2016. The protein files (PDB 5MHP and 5L0K) were obtained
40
41 from Protein Data Bank (<http://www.rcsb.org/pdb/>). The complex was prepared through several steps, such as delete waters
42
43 beyond 0 Å and analyze the work space. The complex was then split into ligands, water, other. Subsequently, the protein
44
45 model was created a binding grid within 15 Å radius around the reference ligand (GLPG-1690). GLPG-1690, **47**, **59** and
46
47 **66** were drawn with ChemBioDraw 3D and thoroughly minimized by CHARMM force field. Finally, possible
48
49 conformations were searched in the binding site using the Glide protocol in default settings (XP precision). The binding
50
51 results were inspected with Discovery Studio 2016 and the 2D binding mode figure was generated from it. The 3D figures
52
53 were obtained from Pymol (The Pymol Molecular Graphics System, Version 1.4.1. Schrodinger, LLC).

54 AUTHOR INFORMATION

56 Corresponding Author

57
58 *Phone: +86 43520257. Fax: +86 43520257. *E-mail: zhaixin_syphu@126.com. maenlong@hotmail.com.

60 Notes

1
2
3
4 The authors declare no competing financial interest.

5
6 ASSOCIATED CONTENT

7
8 Supporting Information

9 Structural characterization Spectra (¹H and ¹³C NMR spectra, MS spectra) of intermediates and target compounds,
10
11 HPLC purity spectra of representative compounds.

12
13 Molecular formula strings (CSV).

14
15 ACKNOWLEDGMENTS

16
17 This research was supported by National Natural Science Foundation of China (No. 81872751), Development Project
18
19 of Ministry of Education Innovation Team (No. IRT1073) and Technology Innovation Guide Fund of Shenyang
20
21 Pharmaceutical University (No. DFJJ2018201).

22
23 ABBREVIATIONS

24
25 ATX, autotaxin; LPC, lysophosphatidylcholine; LPA, lysophosphatidic acid; GPCR, G-protein coupled receptor; BALF,
26
27 bronchoalveolar lavage fluid; BLM, bleomycin; ENPP, ectonucleotide pyrophosphatase/phosphodiesterase; PDE,
28
29 phosphodiesterase; SMB, somatomedin B; S1P, sphingosine-1-phosphate; DNA, Deoxyribo Nucleic Acid; FS-3,
30
31 fluorogenic substrate 3; H&E stain, hematoxylin/eosin stain; IPF, idiopathic pulmonary fibrosis; PLD, phospholipase D;
32
33 HTS, high throughput screening.

34
35 **Reference**

- 36
37 1. Aikawa, S.; Hashimoto, T.; Kano, K.; Aoki, J. Lysophosphatidic Acid as a Lipid Mediator with Multiple Biological
38
39 Actions. *J Biochem.* **2015**, 157, 81–89.
- 40
41 2. Houben, A.J.; Moolenaar, W.H. Autotaxin and LPA Receptor Signaling in Cancer. *Cancer Metastasis Rev.* **2011**, 30,
42
43 557–565.
- 44
45 3. Willier, S.; Butt, E.; Grunewald, T.G. Lysophosphatidic Acid (LPA) Signaling in Cell Migration and Cancer Invasion:
46
47 A Focused Review and Analysis of LPA Receptor Gene Expression on the Basis of more than 1700 Cancer Microarrays.
48
49 *Biol. Cell* **2013**, 105, 317–333.
- 50
51 4. Tager, A.M.; LaCamera, P.; Shea, B.S.; Campanella, G.S.; Selman, M.; Zhao, Z.; Polosukhin, V.; Wain, J.; Karimi-
52
53 Shah, B.A.; Kim, N.D.; Hart W.K; Pardo A.; Blackwell T.S.; Xu Y.; Chun J.; Luster A.D. The Lysophosphatidic Acid
54
55 Receptor LPA1 Links Pulmonary Fibrosis to Lung Injury by Mediating Fibroblast Recruitment and Vascular Leak. *Nat.*
56
57 *Med.* **2008**, 14, 45–54.
- 58
59 5. Contos, J.J.A.; Fukushima, N.; Weiner, J.A.; Kaushaland, D.; Chun, J. Requirement for the LPA 1 Lysophosphatidic
60
Acid Receptor Gene in Normal Suckling Behavior. *Proc. Natl. Acad. Sci. USA.* **2000**, 97, 13384–13389.

- 1
2
3
4 6. King T.E.; Pardo A.; Selman M.; Idiopathic Pulmonary Fibrosis. *Lancet* **2011**, 378, 1949–1961.
- 5
6 7. Kremer, A.E.; Martens, J.J.W.W.; Kulik, W.; Ruëff, F.; Kuiper, E.M.M.; VanBuuren, H.R.; VanErpecum, K.J.;
7
8 Kondrackiene, J.; Prieto J.; Rust, C.; Geenes, V.L.; Williamson, C.; Moolenaar, W.H.; Beuers, U.; Elferink, R.P.J.O.
9
10 Lysophosphatidic Acid is a Potential Mediator of Cholestatic Pruritus. *Gastroenterology* **2010**, 139, 1008–1018.
- 11
12 8. Thirunavukkarasu, K.; Tan, B.; Swearingen, C.A.; Rocha, G.; Bui, H.H.; McCann, D.J.; Jones, S.B.; Norman, B.H.;
13
14 Pfeifer, L.A.; Saha, J.K. Pharmacological Characterization of a Potent Inhibitor of Autotaxin in Animal Models of
15
16 Inflammatory Bowel Disease and Multiple Sclerosis. *J. Pharmacol. Exp. Ther.* **2016**, 359, 207–214.
- 17
18 9. Sevastou, I.; Kaffe, E.; Mouratis, M.A.; Aidinis, V.; Lysoglycerophospholipids in Chronic Inflammatory Disorders: the
19
20 PLA2/LPC and ATX/LPA Axes. *Biochim. Biophys. Acta* **2013**, 1831, 42–60.
- 21
22 10. Umezu-Goto, M.; Kishi, Y.; Taira, A.; Hama, K.; Dohmae, N.; Takio, K.; Yamori, T.; Mills, G.B.; Inoue, K.; Aoki, J.;
23
24 Arai H. Autotaxin Has Lysophospholipase D Activity Leading to Tumor Cell Growth and Motility by Lysophosphatidic
25
26 Acid Production. *J. Cell Biol.* **2002**, 158, 227–233.
- 27
28 11. Tokumura, A.; Majima, E.; Kariya, Y.; Tominaga, K.; Kogure, K.; Yasuda, K.; Fukuzawa, K. Identification of Human
29
30 Plasma Lysophospholipase D, a Lysophosphatidic Acid-producing Enzyme, as Autotaxin, a Multifunctional
31
32 Phosphodiesterase. *J. Biol. Chem.* **2002**, 277, 39436–39442.
- 33
34 12. Hausmann, J.; Keune, W.-J.; HipgraveEderveen, A.L.; van Zeijl, L.; Joosten, R.P.; Perrakis, A. Structural Snapshots of
35
36 the Catalytic Cycle of the Phosphodiesterase Autotaxin. *J. Struct. Biol.* **2016**, 195, 199–206.
- 37
38 13. Nishimasu, H.; Okudaira, S.; Hama, K.; Mihara, E.; Dohmae, N.; Inoue, A.; Ishitani, R.; Takagi, J.; Aoki, J.; Nureki,
39
40 O. Crystal Structure of Autotaxin and Insight into GPCR Activation by Lipid Mediators. *Nat. Struct. Mol. Biol.* **2011**, 18,
41
42 205–212.
- 43
44 14. Salgado-Polo F.; Fish A.; Matsoukas M.T.; Heidebrecht T.; Keune W.J.; Perrakis A. Lysophosphatidic Acid Produced
45
46 by Autotaxin Acts as an Allosteric Modulator of its Catalytic Efficiency, *J. Biol. Chem.* **2018**, 293(37), 14312–14327.
- 47
48 15. Joncour, A.; Desroy, N.; Housseman, C.; Bock, X.; Bienvenu, N.; Cherel, L.; Labeguere, V.; Peixoto, C.; Annoot, D.;
49
50 Lepissier, L.; Heiermann, J.; Hengeveld, W.J.; Pilzak, G.; Monjardet, A.; Wakselman, E.; Roncoroni, V.; Tallec, S.L.;
51
52 Galien, R.; David, C.; Vandervoort, N.; Christophe, T.; Conrath, K.; Jans, M.; Wohlkonig, A.; Soror, S.; Steyaert, J.;
53
54 Touitou, R.; Fleury, D.; Vercheval, L.; Mollat, P.; Triballeau, N.; van der Aar, E.; Brys, R.; Heckmann, B. Discovery,
55
56 Structure-Activity Relationship and Binding Mode of Imidazo[1,2-*a*]pyridine Series of Autotaxin Inhibitors. *J. Med. Chem.*
57
58 **2017**, 60 (17), 7371–7392.
- 59
60 16. Aoki, J.; Taira, A.; Takanezawa, Y.; Kishi, Y.; Hama, K.; Kishimoto, T.; Mizuno, K.; Saku, K.; Taguchi, R.; Arai, H.
Serum Lysophosphatidic Acid is Produced through Diverse Phospholipase Pathways. *J. Biol. Chem.* **2002**, 277, 48737–

1
2
3
4 48744.

5 17. Lynch, K.R.; Macdonald, T.L. Phosphonate Derivatives as Autotaxin Inhibitors. US 8378100, Feb 19, 2013.

6
7 18. Kato, K.; Ikeda, H.; Miyakawa, S.; Futakawa, S.; Nonaka, Y.; Fujiwara, M.; Okudaira, S.; Kano, K.; Aoki, J.; Morita,
8 J.; Structural Basis for Specific Inhibition of Autotaxin by a DNA Aptamer. *Nat. Struct. Mol. Biol.* **2016**, *23*, 395–401.

9
10 19. Barbayianni, E.; Kaffe, E.; Aidinis, V.; Kokotos, G. Autotaxin, a Secreted Lysophospholipase D, as a Promising
11 Therapeutic Target in Chronic Inflammation and Cancer. *Progr. Lipid Res.* **2015**, *58*, 76-96.

12
13 20. Nikolaou, A.; Kokotou, M. G.; Linnios, D.; Psarra, A.; Kokotos, G. Autotaxin Inhibitors: a Patent Review (2012–2016).
14 *Expert Opin. Ther. Pat.* **2017**, *27*, 815–829.

15
16 21. Gierse, J.; Thorarensen, A.; Beltey, K.; Bradshaw-Pierce, E.; Cortes-Burgos, L.; Hall, T.; Johnston, A.; Murphy, M.;
17 Nemirovskiy, O.; Ogawa, S.; Pegg, L.; Pelc, M.; Prinsen, M.; Schnute, M.; Wendling, J.; Wene, S.; Weinberg, Robin.;
18 Wittwer, A.; Zweifel, B.; Masferrer, J.; A novel Autotaxin Inhibitor Reduces Lysophosphatidic Acid Levels in Plasma and
19 the Site of Inflammation. *J. Pharmacol. Exp. Ther.* **2010**, *334*, 310-317.

20
21 22. Desroy, N.; Housseman, C.; Bock, X.; Joncour, A.; Bienvenu, N.; Cherel, L.; Labeguere, V.; Rondet, E.; Peixoto, C.;
22 Grassot, J. M.; Picolet, O.; Annoot, D.; Triballeau, N.; Monjardet, A.; Wakselman, E.; Roncoroni, V.; Tallec, S. L.; Blanque,
23 R.; Cottereaux, C.; Vandervoort, N.; Christophe, T.; Mollat, P.; Lamers, M.; Auberval, M.; Hrvacic, B.; Ralic, J.; Oste, L.;
24 van der Aar, E.; Brys, R.; Heckmann, B. Discovery of 2-[[[2-Ethyl-6-[4-[2-(3- hydroxyazetidid-1-yl)-2-oxo-
25 ethyl]piperazin-1-yl]-8-methylimidazo[1,2-a]pyridin-3-yl]methylamino]-4-(4-fluorophenyl)thiazole-5-carbonitrile
26 (GLPG1690), a First-in-Class Autotaxin Inhibitor Undergoing Clinical Evaluation for the Treatment of Idiopathic
27 Pulmonary Fibrosis. *J. Med. Chem.* **2017**, *60* (9), 3580-3590.

28
29 23. Howard, H.J.; Andrew, P.T.; Duane, B.K.; David, L. Heterocyclic Vinyl Autotaxin Inhibitor Compounds.
30 WO2015042052A1, Mar 26, 2015.

31
32 24. Frances, E.J. Methods and Compositions for the Treatment of Metabolic Disorders. WO2016028686A1, Feb 25, 2016.

33
34 25. Stein, A.J.; Bain, G.; Prodanovich, P.; Santini, A.M.; Darlington, J.; Stelzer, N.M.P.; Sidhu, R.S.; Schaub, J.; Goulet,
35 L.; Lonergan, D.; Calderon, I.; Evans, J.F.; Hutchinson, J.H. Structural Basis for Inhibition of Human Autotaxin by Four
36 Potent Compounds with Distinct Modes of Binding, *Mol. Pharmacol.* **2015**, *88*, 982-992.

37
38 26. Nikolaou, A.; Ninou, I.; Kokotou, M. G.; Kaffe, E.; Afantitis, A.; Aidinis, V.; Kokotos, G.; Hydroxamic Acids Constitute
39 a Novel Class of Autotaxin Inhibitors that Exhibit *in Vivo* Efficacy in a Pulmonary Fibrosis Model, *J. Med. Chem.* **2018**,
40 *61*, 3697–3711.

41
42 27. van der Aar, E.; Desrivot, J.; Dupont, S.; Heckmann, B.; Fieuw, A.; Stutvoet, S.; Fagard, L.; Van de Wal, K.; Helmer,
43 E. Safety, Pharmacokinetics, and Pharmacodynamics of the Autotaxin Inhibitor GLPG1690 in Healthy Subjects: Phase 1
44
45
46
47
48
49
50
51
52
53
54
55
56
57
58
59
60

1
2
3
4 Randomized Trials. *J Clin. Pharmacol.* **2019**, 00, 1–14.

5
6 28. Maher, T.M.; van der Aar, E.M.; Van de Steen, O.; Allamassey, L.; Desrivot, J.; Dupont, S.; Fagard, L.; Ford, P.; Fieuw,
7
8 A.; Wuyts, W. Safety, Tolerability, Pharmacokinetics, and Pharmacodynamics of GLPG1690, a Novel Autotaxin Inhibitor,
9
10 to Treat Idiopathic Pulmonary Fibrosis (FLORA): A Phase 2a Randomized Placebo-controlled Trial. *Lancet Respir. Med.*
11
12 **2018**, 6, 627-635.

13
14 29. Maher, T.M.; Kreuter, M.; Lederer, D.J.; Brown, K.K.; Wuyts, W.; Verbruggen, N.; Stutvoet, S.; Fieuw, A.; Ford, P.;
15
16 Abi-Saab, W.; Wijssenbeek, M. Rationale, Design and Objectives of Two Phase III, Randomised, Placebo Controlled Studies
17
18 of GLPG1690, a Novel Autotaxin Inhibitor, in Idiopathic Pulmonary Fibrosis (ISABELA 1 and 2). *BMJ Open Resp. Res.*
19
20 **2019**, 6, e000422.

21
22 30. The websites for predicting general molecular properties: <http://swissadme.ch/index.php>; <http://www.molsoft.com>

23
24 31. Hopkins, A.L.; Keserü, G.M.; Leeson, P.D.; Rees, D.C.; Reynolds, C.H. The role of ligand efficiency metrics in drug
25
26 discovery. *Nat Rev Drug Discov*, **2014**, 13(2), 105–121.

27
28 32. Edwards, M.P.; Price, D.A. Role of Physicochemical Properties and Ligand Lipophilicity Efficiency in Addressing
29
30 Drug Safety Risks, *Annu Rep Med Chem*, **2010**, 45, 380-391.

31
32 33. Moeller, A.; Ask, K.; Warburton, D.; Gauldie, J.; Kolb, M. The Bleomycin Animal Model: a Useful Tool to Investigate
33
34 Treatment Options for Idiopathic Pulmonary Fibrosis? *Int. J. Biochem. Cell Biol.* **2008**, 40,362–382.

35
36 34. Oikonomou, N.; Mouratis, M. A.; Tzouvelekis, A.; Kaffe, E.; Valavanis, C.; Vilaras, G.; Karameris, A.; Prestwich, G.
37
38 D.; Bouros, D.; Aidinis, V. Pulmonary Autotaxin Expression Contributes to the Pathogenesis of Pulmonary Fibrosis. *Am.*
39
40 *J. Respir. Cell Mol. Biol.* **2012**, 47, 566–574.

41
42 35. Ninoua, I.; Kaffe, E.; Müllerb, S.; Budde, D.C.; Stevenson, C.S. Ullmerb, C.; Aidinisa, V. Pharmacologic Targeting
43
44 of the ATX/LPA Axis Attenuates Bleomycin-induced Pulmonary Fibrosis. *Pulm. Pharmacol. Ther.* **2018**, 52, 32–40.

45
46 36. Ashcroft, T.; Simpson, J.M.; Timbrell, v. Simple Method of Estimating Severity of Pulmonary Fibrosis on A numerical
47
48 Scale. *J. Clin.Pathol.* **1988**, 41, 467-470.

49
50 37. Hübner, R.H.; Gitter, W.; Mokhtari, N.E.E.; Mathiak, M.; Both, M.; Bolte, H.; Freitag-Wolf, S.; Bewig, B. Standardized
51
52 Quantification of Pulmonary Fibrosis in Histological Samples. *BioTechniques* **2008**, 44, 507-517.

53
54 38. Katsifa, A.; Kaffe, E.; Nikolaidou-Katsaridou, N.; Economides, A.N.; Newbigging, S.; McKerlie, C.; Aidinis, V. The
55
56 Bulk of Autotaxin Activity Is Dispensable for Adult Mouse Life. *PLoS One* **2015**, 10, e0143083.

57
58 39. Wang, Y.; Chen, S.W.; Hu, G.; Wang, J.; Gou, W.F.; Zuo, D.Y.; Gu, Y.C.; Gong, P.; Zhai, X.; Discovery of Novel 2,4-
59
60 Diarylaminopyrimidine Analogues as ALK and ROS1 Dual Inhibitors to Overcome Crizotinib-resistant Mutants Including
G1202R. *Eur. J. Med. Chem.* **2018**, 143 123-136.

- 1
2
3
4 40. Yao, S.J.; Ren, Z.H.; Wang, Y.Y.; Guan, Z.H.; Friedel–Crafts Fluoroacetylation of Indoles with Fluorinated Acetic
5
6 Acids for the Synthesis of Fluoromethyl Indol-3-yl Ketones under Catalyst- and Additive-Free Conditions. *J. Org. Chem.*
7
8 **2016**, 81, 4226–4234.
- 9
10 41. Lepri, S.; Buonerba, F.; Goracci, L.; Velilla, I.; Ruzziconi, R.; Schindler, B.D.; Seo, S.M.; Kaatz, G.W.; Cruciani, G.
11
12 Indole Based Weapons to Fight Antibiotic Resistance: A Structure–Activity Relationship Study. *J. Med. Chem.* **2016**, 59,
13
14 867–891
- 15
16 42. Maiti, A.; Reddy, P.V.N.; Sturdy, M.; Marler, L.; Pegan, S.D.; Mesecar, A.D.; Pezzuto, J.M.; Cushman, M. Synthesis of
17
18 Casimiroin and Optimization of Its Quinone Reductase 2 and Aromatase Inhibitory Activities, *J. Med. Chem.* **2009**, 52,
19
20 1873–1884.
- 21
22
23
24
25
26
27
28
29
30
31
32
33
34
35
36
37
38
39
40
41
42
43
44
45
46
47
48
49
50
51

52 Table of Contents graphic
53
54
55
56
57
58
59
60

